POLITECNICO DI MILANO

SCUOLA DI INGEGNERIA CIVILE, AMBIENTALE E TERRITORIALE

Corso di Laurea Magistrale in Ingegneria Civile

ONE WAY FLUID STRUCTURAL INTERACTION FOR GREENVALVE'S ROTOR BLADES ANALYSIS

Tesi di laurea di :
Olivier BACCINO
Matr. 817453

Relatore : Prof. Ing. Stefano MALAVASI
Correlatore : Ing. Giacomo FERRARESE

Anno Accademico 2014 - 2015

ONE WAY FLUID STRUCTURAL INTERACTION FOR GREENVALVE'S ROTOR BLADES ANALYSIS

Olivier Baccino

Politecnico di Milano

Abstract

In a world where energy harvesting is becoming one of the challenges of tomorrow, the GreenValve, which is originally a control valve, relies on converting energy from fluid flowing through water utilities into a reusable mechanical energy. For the purpose of investigating a possible turbine geometry, numerical simulations had been carried out to evaluate characteristics of NACA0040 airfoil profile blades that compose the GreenValve's turbine, mainly in a confined environment, through a One Way FSI Analysis.

Using ANSYS Fluent, with a Realizable κ-ϵ turbulence model, simulations have been performed to understand the fluid behavior, impacted by its surrounding environment, with a Reynolds number of 50 000. From these have been reached drag and lift coefficients, as well as the moment developed by the turbine, for several positions of the turbine's blades. 2D and 3D models have been performed to realize that these parameters do not depend on the dimension of the problem.

After CFD simulations, the flow field solutions obtained have been transferred to the solids surfaces to calculate constraints and deformations on the thermoplastic turbine, for different valve apertures. It results that from these few investigated configurations, the field of constraints significantly increases when the valve is closing, up to a point where the turbine suffers from irreversible damages. Then, alternative turbine configurations, as well as different fluid velocity inlets and the determination of the maximum differential pressure achievable, have been explored, to reduce mechanical constraints and to lead to a more adequate geometry for the whole valve.

Ma oggi che tutto è finito, che di tanto male, di tanto bene non rimane che cenere, posso raccontare la sua avventura singolare.
Alain Fournier

Contents

List of Figures

List of Tables

Introduction

During the past few years, renewable energies have become a new challenge to overcome, an alternative to fossil fuels energy's shortage and a way to cope with climate change and greenhouse effects. Among these new sources of energy, wind energy, and in a more general way, energy extracted from fluid displacements, could constitute a solid alternative.

The GreenValve concept is one of them; it is a control valve able to recover energy from processes that naturally require energy dissipation. In order to optimize the amount of energy recovered through the GreenValve process, it must be understood how the fluid-structure interaction works in a confined environment. To this aim, the fluid behavior into the tube, and how it is affected by the presence of the turbine, spinning inside the valve, will be investigated. Reciprocally, the latter will also influence the structural behavior of the turbine, which is part of the GreenValve.

In this work, a possible turbine geometry - in which the blades were designed as NACA 0040 airfoil profiles - but not the best, have been investigated on a structural level, to check the pressure that is achievable for that geometry. All along this study, the turbine will be composed by three blades, making an angle of 120° to each other.
All the simulations will be performed through Fluent, using steady-state solver, with a Realizable κ-ϵ turbulence model.
The confined environment and a Reynolds number of 50 000 make the study framework slightly different to what can be found in the literature. Yet, several models will be investigated to understand how different conditions can affect the studied parameters, namely the drag and lift coefficients, the moment developed by the turbine and the flow coefficient. Different positions of the blades, *i.e.* different angles of attack, will be considered, in order to cover the whole blades positions range. Among these different models, two dimensional models will be developed and compared to cases in which the airfoil is surrounded, whether by a confined environment or an unconfined one. In addition, the influence of the blades on each other will be a matter of importance, and cases in which only a single blade stands inside the tube will be regarded, as well as when the three blades composing the turbine lie inside the tube. Afterwards, three dimensional simulations will be performed and compared to the results obtained for the two dimensional ones. Mainly two different cases will be treated in this part : as the plane along the tube's length is a symmetrical axis, a half section of it will be considered to save some computational time. Then, a smaller part of this section will be also explored, in order to see whether the drag and lift coefficients, and the moment developed by the turbine, are affected by these simplifying choices.

Furthermore, the GreenValve is willing to be used as an On/Off valve, and one of the

objectives is to increase the flow coefficient with respect to the standard GreenValve, which had been experimentally tested at the laboratory of the Politecnico di Milano. Being not only designed to recover energy, but also as a control valve, this additional characteristic means that its aperture ought to be monitored to control parameters such as flow rate. As the valve must be naturally moved between opened and closed positions, these intermediate positions will be also investigated, as they're probably the most dangerous positions for the turbine, and have a major structural influence on the valve, which has to be carefully inspected.

The interaction between the fluid and the structure will be performed, coupling results from the CFD to the structural part. This way, informations will be obtained regarding the ability of the turbine, made of a thermoplastic material, to remain in the elastic domain. Deformation and strain will be also examined, and geometric modifications will be tested, to try to improve the mechanical resistance of the structure, based on the pressure drop.

Chapter 1

Context of the thesis

Recovering energy from environmental sources is becoming one of the most important challenges for the following years. In this chapter will be introduced several solutions which have been developed along the years to take advantage of the wind, that is one of the most promising renewable source to produce energy.

In addition, the GreenValve, a control valve developed at the Politecnico di Milano, will be specifically introduced.

1.1 Overview of the existing technology

One of the few methods recently developed is to generate power from a turbine set inside a pipe, when water flows through this latter. For instance, the LucidPipe, which is presented in the figure below, is based on this approach. The turbine is a lift-based one, which extracts very little head pressure; it has a negligible impact on the pipeline efficiency, and can generate power across a very wide range of velocities.

Figure 1.1: LucidPipe^{TM} Power System

The GreenValve project involves a very similar principle which will later be explained.

Yet, few general considerations will be made about the several types of turbines (Generally most suitable for wind) that can be found in the literature.

There are two main types of wind turbines :

- Horizontal Axis Wind Turbine (HAWT)
- Vertical Axis Wind Turbine (VAWT)

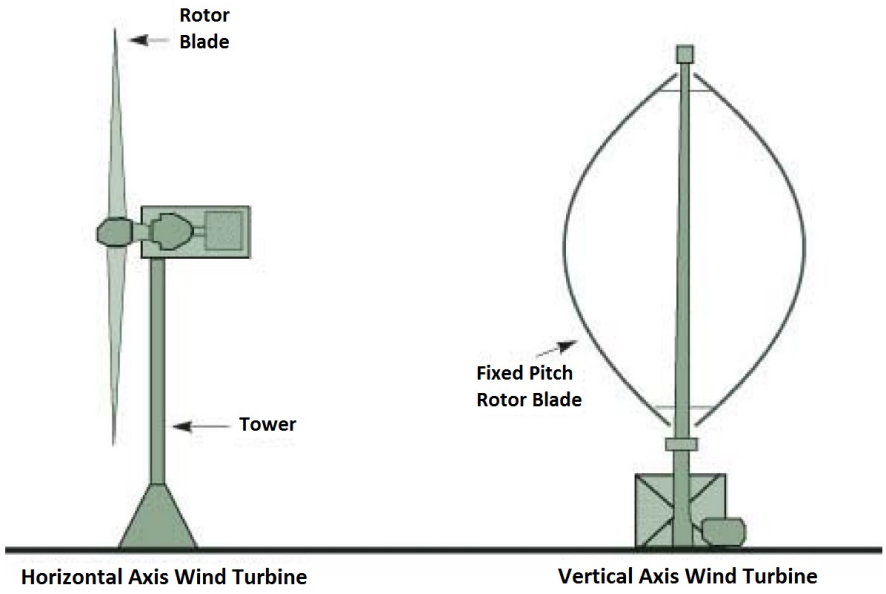

Figure 1.2: Schematic diagrams of the two types of wind turbines

HAWTs have been massively studied, to evolve into a mature technology for converting wind power into electricity, thanks to its sufficient enough efficiency. On the other hand, VAWTs have not been studied much, because ofhe fact they are less efficient than HAWTs. However, VAWTs have many advantages that should not been neglected : they have low production and affordable maintenance costs . In addition, they can produce energy independently of the direction of the wind, and in turbulent and unstructured flows; they are not subject to so much variations of the power coefficient

VAWTs also present the advantage of being constituted of constant blade shapes along the radius direction, which makes them easier to manufacture.

Regarding the environment in which these turbines are used, water utilities (but also other fluid plants) are mainly used to ensure safe and clean water supply, by efficiently controlling water quality, and managing its pressure distribution. These controlling devices, to get all the different data, are powered by batteries, which are hard to reach once settled on, and have quite a short operational period.

Different problematics have then been developed to recuperate energy from fluids running through the pipelines, not only to power controlling devices, but also to use it as an alternative source of energy. Among these, the GreenValve has been developed and experimentally tested, in order to convert this energy into a mechanical one. It constitutes both a flow control valve and an energy harvesting turbine. Prototypes tested at the Politecnico

di Milano have been made using turbines of different blade shape in order to give an idea of the flow coefficient and the efficiency retrieved from these devices.

1.1.1 Numerical approach

From a numerical point of view, the development of the CFD (Computational Fluid Dynamic) has led to highly accurate models. It has become an attractive method to provide an essential contribution to the development of the VAWTs. Among these, studies on blade shapes have been realized, but mainly cases in which the fluid treated was the air. Multiple-blade turbines have been put into a duct, in order to give more velocity to the flow upstream of the turbine. The optimization is based on several parameters such as chord length, rotor diameter, pitch angle, blade thickness ratio and helical angle. Numerical studies are made using a commercial software such as ANSYS FLUENT®. To simulate the behavior of the structure submitted to fluid interaction, a one-way fluid-structure interaction has been used. It consists of a first step to simulate the behavior of the fluid inside the duct, and then, using these results, applying them to the structural part, that is to say to the turbine, in order to understand how the fluid affects its performance.

The choice of the blade shape is made by selecting the most accurate NACA (National Advisory Committee for Aeronautics) airfoil, with reference to its characteristics.

1.1.2 NACA profiles

The NACA profiles are airfoil shapes for aircraft wings developed mainly for the aeronautic domain. Their geometry is summed up using a series of digits following the word NACA, which makes it possible to define exactly the airfoil considered. For the cases studied, four digits series, for symmetric airfoil shapes, are used. This can be written as follow : NACA MPXX

Where :

- M describes the maximum camber as a percentage of the chord: 100m=M
- P describes the distance of maximum camber from the airfoil's leading edge in tens of percents of the chord: 10p=P
- The last two digits describe the maximum thickness of the airfoil as a percentage of the chord: 100t=XX

To give an example, the NACA 0040 profile is drawn in the following figure. The 00 indicates that this profile has no camber, and the 40 means that the airfoil has a 40% thickness to chord length ratio : it is 40% as thick as it is long.
More informations can be found in [19] about this profiles, which will be used to model GreenValve's blades along this thesis.

In the following part, the Vertical Axis Wind Turbines will be more precisely described, as this type of turbines constitutes one of the fundamental principles of the GreenValve, it must be understood what phenomenon makes it work.

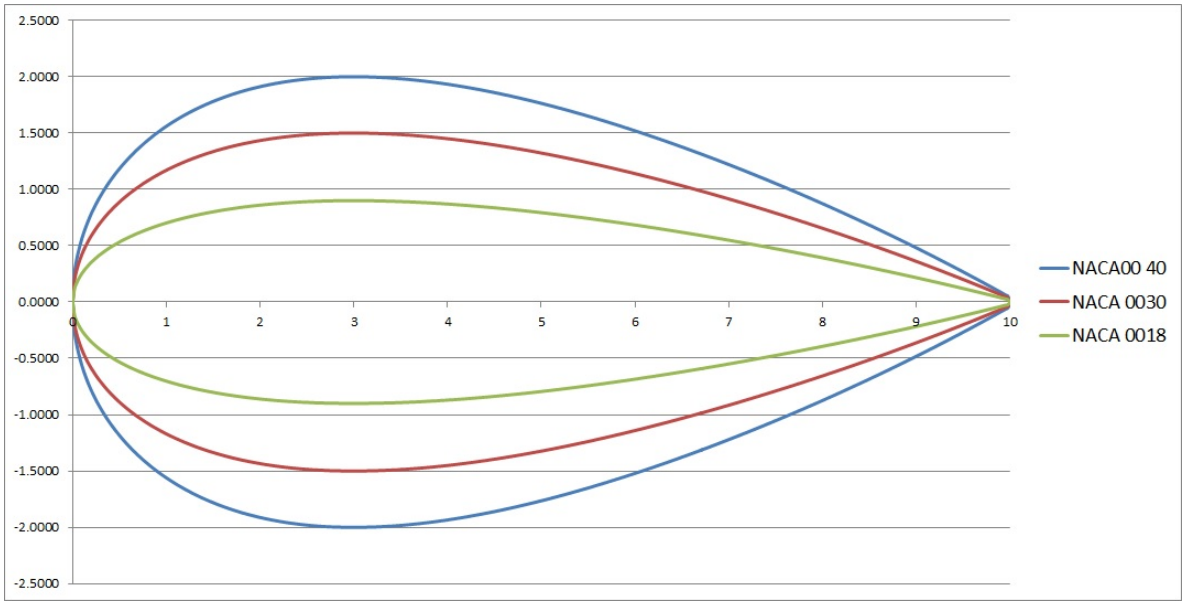

Figure 1.3: Several NACA profiles

1.2 Vertical Axis Wind Turbines

As said previously, Vertical Axis Wind Turbines can have many important advantages in the actual market, compared to Horizontal Axis Wind Turbines. The characteristics of these turbines will be discussed in this section.
Unlike Horizontal Axis Wind Turbines (HAWTs), which have already been widely studied in the past, and applied to large-scale power plants, there are not many studies on VAWTs, mainly because they are less efficient than HAWT.
However, VAWTs are currently receiving an increasing interest because their turbine typology constitutes one of the most suitable solutions in non-conventional installation areas (Cf. [3], [5], [7], [8], [16]).
In fact, one of the main advantages of Vertical Axis Wind Turbines is that, due to their geometry, the direction of the wind does not have any influence on the production rate of energy. Moreover, unlike for the HAWTs, a generator can be located wherever along its vertical axis, which gives the possibility to place it to get an easy access to it. For instance, considering a submarine turbine, the electrical part can be put above the water surface.

There are two main types of VAWTs :

- Drag-type (Savonius)
- Lift–type (Darrieus)

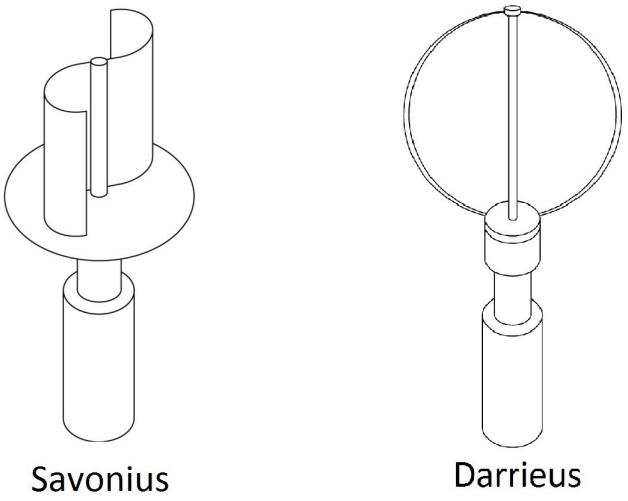

Figure 1.4: Savonius and Darrieus turbines

1.2.1 Savonius turbine

The Savonius turbine is a drag-type device, constituted of at least two coops, slightly out of alignment. These two coops are put in such a way that it creates a differential drag (the scoop is subject to more drag when moving with the wind and to less drag when moving against the wind) which makes the turbine to spin. Yet, the efficiency of this type of VAWT is lesser than that other types, such as lift-type devices. It is then mainly used for cases in which efficiency is not the most important parameter, like for anemometers.

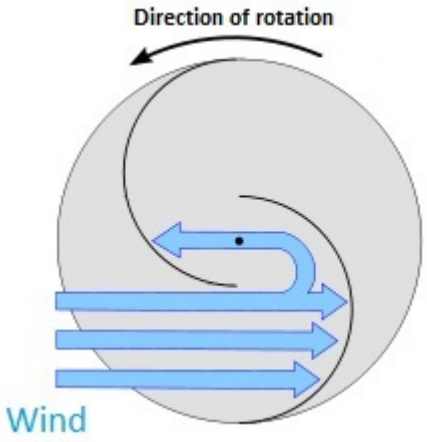

Figure 1.5: Savonius principle

1.2.2 Darrieus turbine

The Darrieus turbine is a lift-type device. For an airfoil subject to an airflow, it is submitted, depending on the angle of the blades, to different forces, with different intensities and directions (lift and drag). In the case of Darrieus turbines, the drag has a negative impact on the rotation of the blades, and then on the efficiency of the turbine. On the contrary, the lift force has a positive impact on the rotation. It is then very important to optimize the airfoil profile chosen, in order to tend to have a higher lift-force than drag-force.

This the most common type of turbine used for power generation from water pipelines ([1], [2], [3], [5], [7], [8], [16]).

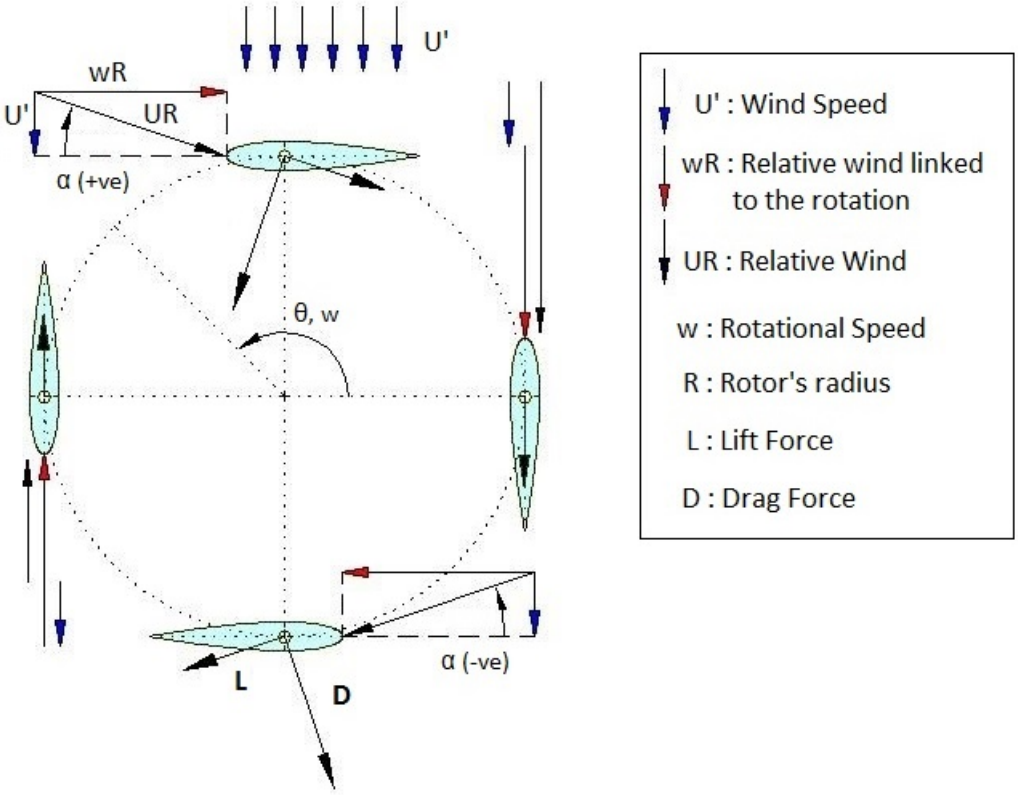

Figure 1.6: Darrieus principle

1.3 Control Valves

Control valves are used to control conditions such as flow, pressure, temperature, and liquid level which are passing through it, by controlling valve aperture with respect to signals received from controllers. The valve plug is attached to a valve stem, which, in turn, is connected to the actuator. The actuator, that can be pneumatically or electrically operated, directs the movement of the stem as dictated by the external control device. The

control valve is then the final control element of the control loop.
Thanks to this, the pressure drop in the valve can be regulated when the fluid crosses the latter, and as a consequence, the flow rate is possibly controlled .

A standard control valve is composed by three main parts :

- The valve actuator : Coupled to the body part thanks to a rod; its goal is to shift the valve by giving a command order.
- The valve positioner : To enslave the position of the obturator, providing for the actuator the necessary driving force to come through friction forces.
- The valve body : Mounted in series in the pipeline, contains the valve itself.

Figure 1.7: Control Valve

1.4 Flow Coefficient

The control valve capacity depends directly on the flow coefficient C_v, which defines the relation between the flow rate Q and the pressure drop Δp existent for a specific configuration of the tested device. Its most common function is to measure the expected pressure loss across the valve. This makes it possible to compare the flow efficiency of valves at different sizes or types, in order to select the most suitable one for any specific application. It is expressed as :

$$C_v = \frac{Q}{N_1 \sqrt{\frac{\Delta p}{\rho / \rho_0}}}$$

Where :

- Q is the flow rate in m^3/hour
- Δp is the pressure drop in bar
- ρ/ρ_0 is the specific gravity of fluid
- N_1 is a transformation parameter equal to 0,895 in order to obtain C_v in GPM/$psi^{0,5}$

There are different ways to express the value of the flow coefficient (C_v) (Also known as Flow factor (K_v)) whether we consider the European normative one, the American one or the Anglo-Saxon one. In the European normative one, the flow rate is expressed in cubic meters per hour (m^3/hour), the pressure in bar and then K_v in $m^3/hour$.
Conversely, in the American normative, the flow rate is expressed in GPM (Gallons per minute) and the Pressure drop across valve is in psi (1 psi=6895 Pa). Then, C_v is in $psi^{-1/2}GPM^{-1}$.
In Anglo-Saxon, the reference is made to the Flow Coefficient (C_v), which corresponds to a rate of flow (US gallons per minute) at 60 $^\circ$F which goes through a valve with a pressure drop of 1 psi across the valve.
These two coefficients are connected by the following equation :

$$K_v = 0,865 C_v$$

1.5 The GreenValve

The principle of the GreenValve comes from a relatively simple observation : Energy which passes through pipelines or other types of tubes in which fluids (Liquid or gas) are present, is wasted. Then, the idea is to save this energy, by converting it into a mechanical one that can be directly used or transformed. Moreover, and unlike the other recovering energy devices already existing, the GreenValve is capable of both controlling the flow and recovering energy at the same time. It works as an On/Off valve, which means that there are only two positions for which it can be used : fully opened or completely closed.

The GreenValve represents a direct application of the so-called Energy Harvesting process.

This technique consists in getting energy from external sources (*e.g.* solar power, thermal energy, wind energy...), captured, and stored for small, wireless autonomous devices.

In fact, the amount of energy recoverable, for instance, from an aqueduct, could represent about 60-100 MWh/year, which is equivalent to the annual use of 17 to 28 European average families.

Figure 1.8: GreenValve Prototype

All that have been described in this section leads to a better understanding of the physical phenomenon involved in the behavior of a wind turbine, whether with a vertical axis or an horizontal one. Moreover, it introduces us to the GreenValve, whose structural behavior will constitute the central part of this thesis.

Chapter 2

Numerical simulations, use of CFD

Numerical simulations will constitute an essential tool to proceed to the structural verifications and design of the GreenValve. Its process must be understood in its wholeness to take full advantage of it.

2.1 Design methodology

The development of the CFD opened a new era in the fluid dynamic domain. In fact, design has evolved from mainly experimental tests to a mainly computational design, verified then by experimental tests. CFD is cheaper and allows a deeper inspection of the design possibilities. As a consequence, costs design have been reduced, as the number of experimental tests made (They are only realized when relevant computational results are obtained).

The several steps which constitute the design methodology of a model that couples fluid dynamics analysis to mechanical behavior of a system can be summed up as :

- A first CAD model is designed on a CAD Software such as SolidWorks or Catia
- The CAD model is imported on a CFD Software like Fluent, in which the fluid action will be simulated
- If simulation results match the expected objectives of the design process, there is no need to modify it.
- If not, by taking into account the previous results, the CAD model is modified in improved and order to be more accurate than the latter one.
- This loop-through is repeated until simulation results jibe with the objectives.

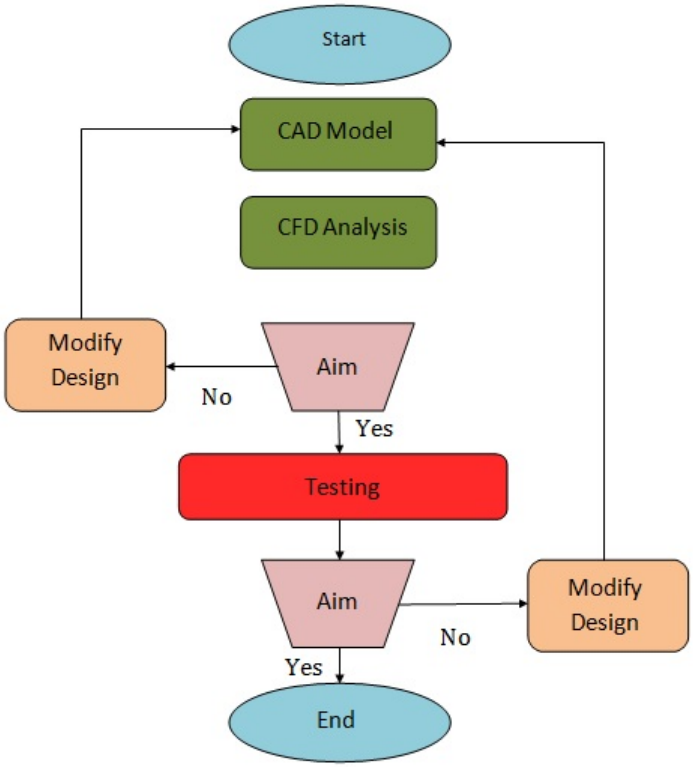

Figure 2.1: Design methodology

2.2 CFD settings

To model the interaction between a fluid flow and a structure, one has to be careful of which settings are adopted for the simulations. In the case of a fluid flow going through a turbine, it has to be chosen between a steady or an unsteady flow field. The steady state means that the flow characteristics do not vary in time, and then, the unsteady state means this latter vary in time.

At this point, there are two ways to simulate the problem, making an URANS (Unsteady Reynolds Average Naver-Stokes) simulations or a RANS one. URANS simulations are quite time consuming compared to steady RANS simulations. Nevertheless, the used method strictly depends on the problem studied, and the parameter examined.

All simulations performed in the following will be RANS ones.

In addition, concerning the mesh, a sliding mesh method must be adopted in order to performed the rotation of the turbine and simulate its behavior correctly. Actually, the part of the fluid flow mesh located in the internal part of the turbine diameter must be considered as moving relatively to the other zones of the mesh. Yet, the first part of the study will concern only fixed position of the turbine, which let us mesh the whole domain in an uniform way.

Concerning the mesh, the tetrahedrons assembly meshing has been used. In addition, boundary layers (also known as inflation) have been added around the structural part,

that is to say the turbine, and along the tubes wall. In fact, boundary layers must be added in regions where the flow will experience rapid change in key variables such as pressure, velocity or temperature.

2.3 Computational domain

The computational domain has to be properly defined in order to save computational time (Not too large) and also to get accurate results (Not too small).

The density of the grid has a significant impact on the accuracy of the solution. It has to be chosen carefully. To know how many grids have to compose the model, several models must be made, changing the size of the grid. When considered parameters become independent of the grid number, it means that our model is stable. Of course, the more meshes are fine, the more accurate the solution is. Yet, it must be considered that from a certain grid number, the solution does not significantly evolves, and it makes us save an important computational time.

2.4 Turbulence model

Two models are mainly use in CFD simulation of VAWTs. Most common simulations have been summed up in [10]. It can be observed that both κ-ϵ and κ-ω turbulence models are widely used in the literature. Yet, when a 3D model is used, κ-ϵ turbulence models are always the ones considered. In the following, only the Realizable κ-ϵ one will be considered, because it gives a better numerical stability, according to [16]. Yet, even if some 2D simulations will be performed, one needs to bear in mind that topics of this thesis must be developed through a three-dimensional approach. Then, even for 2D simulations, the Realizable κ-ϵ model will be used.
Besides, any consideration based on the literature, advantages and disadvantages of each model must be understood, on the mathematical level.

2.5 Dimensionless wall distance y^+

y^+ was first introduced by V. Karman for the universal law of the wall for turbulent wall boundary layers. In CFD, the use of y^+ in turbulence models is required to evaluate the wall distance which represents the influence of the Reynolds stress tensor. It can be expressed as follow : $y^+ = \frac{u_* * y}{\nu}$

Where:

- u_* is called the friction velocity or shear velocity
- y is the distance to the nearest wall
- ν is the local kinematic viscosity of the fluid.

The use of y^+ is an indicator to verify if the boundary layer is sized well.

2.6 One-Way Fluid-Structure Interaction (FSI)

One-way FSI (Fluid Structure Interaction) is developed to facilitate interaction between Fluids and structure as it is often used together. It makes possible to apply results of fluid analysis (temperatures, pressures...) to structural analysis using them as boundary conditions. This way, solid surfaces constitute interfaces between the fluid and solid domains, which makes possible to transfer mechanical loads from a CFD analysis to a mechanical solver.

In our case, each pressure load will be applied on the part it is actually acting on, which will make possible to observe the structural behavior of each component independently of the others .

One-way FSI provides an economic alternative, but does not take into account the modification of any of the meshes. (unlike the two-ways FSI which includes an iterative loop between both CFD and mechanical models, in which the structual response does affect the fluid motion).

Chapter 3

Theory used to solve numerical problems

Computational Fluid Dynamic constitutes a strong tool to model all kinds of fluid problems. The completeness of this method comes with a high complexity and the necessity to use mathematic models that actually correspond to the physical problem we're dealing with.

Hence, it is important to seize the core of the mechanisms that control it, that is to say the theoretical meanings of the fluid mechanic equations and of few several turbulence models that can be employed with respect to the problem we're dealing with.

3.1 Fluid Mechanics Equations

Fluid Dynamic is the study of fluids in motion. The basic equations governing fluid motion are known as the incompressible Navier-Stokes equations, named after Claude-Louis Navier and George Gabriel Stokes. This is a system of non-linear partial differential equations which can be written as follow :

The instantaneous continuity equation :

$$\frac{\partial \rho}{\partial t} + \frac{\partial}{\partial x_i}(\rho u_i) = 0$$

The momentum equation :

$$\frac{\partial u_i}{\partial t} + u_j \frac{\partial u_i}{\partial x_j} = -\frac{1}{\rho}\frac{\partial p}{\partial x_i} + \nu \frac{\partial^2 u_i}{\partial x_i \partial x_j}$$

Where u_i represents the velocity in the direction i (i$\in$[1;3]), p the static pressure and ν the kinematic viscosity of the fluid, equal to $\nu = \frac{\mu}{\rho}$ (with ρ the density and μ the dynamic viscosity).

The analytical resolution of these non-linear partial differential equations, which depends on the geometry and on the boundary conditions is impossible, except for cases in which simplifications are made, such as laminar flow in a pipe, when the flow can be considered

as one-dimensional.
This is where the use of numerical methods needs to be considered, to solve more complex problems, in which the domain is divided in several different sections (named mesh). Then the non-linear partial differential equations are discretized in order to be numerically solved.

3.2 About CFD

The CFD, *i.e.*"Computational Fluid Dynamics" is a numerical method which enables to obtain an approximate solution of a complex fluid dynamic problem. Then, the principle, is to solve fluid dynamics equations in a numeric way. Nevertheless, the solution is not exact. Why that ?
First and foremost, Navier-Stokes equations are solved by discretizing the problem, which gives rise to a slightly different model compared to the initial one.
Also, because of the limited computing power, few terms of the equations are replaced by empirical models which are obviously not exact. Yet, the current computing power is still sufficient to obtain, through CFD models, highly satisfactory results for industrial purposes.

Among the three ways to deal with a fluid dynamics problem (Analytic, Experimental and Numerical ones), the numerical method requires less hypothesis than the analytic one and makes possible to solve more complex problems. Besides, it is cheaper than an experimental approach. Yet, numerical and experimental approaches are linked together by the fact that these two are complementary. In fact, before every experiment, a CFD study may be performed in order to better understand the problem studied. Reciprocally, the exprimental process aims to better understand CFD results, and to put into perspective choices made concerning the model used. In fact, some of them are more suitable for some types of problems; the choice of the CFD model must take into account the objectives of the simulations.

3.3 Two-equations turbulence models

Models adopted must be the more accurate as possible, to be as near as it can be to the physical reality of our problems. Then, it is important to understand each model properly, to know in which cases they can exploited, their advantages and disadvantages. Two equation turbulence models are one of the most common type of turbulence models used in the industry. It means that these models have 2 extra transport equations to represent the turbulent properties of the flow.

3.3.1 κ-ϵ models

The first transported variable κ concerns the turbulent kinetic energy (which determines the energy of the turbulence), whereas the second transported variable ϵ is attached to the turbulent dissipation (and determines the scale of the turbulence). Two formulations of

κ-ϵ models will be considered in the following, specifically the Standard κ-ϵ model and the Realizable κ-ϵ one.

3.3.1.1 Standard κ-ϵ model

The standard $\kappa - \epsilon$ model is one of the most used model because of its robustness, economy and its acceptable accuracy for a wide range of problems. This model constitutes a semi-empirical model based on two transport equations, which are developed in the following:

For turbulent kinetic energy κ :

$$\frac{\partial}{\partial t}(\rho\kappa) + \frac{\partial}{\partial t}(\rho\kappa u_i) = \frac{\partial}{\partial x_j}[(\mu + \frac{\mu_t}{\sigma_\kappa})\frac{\partial \kappa}{\partial x_j}] + P_\kappa + P_b - \rho\epsilon - Y_M + S_\kappa$$

For dissipation ϵ :

$$\frac{\partial}{\partial t}(\rho\epsilon) + \frac{\partial}{\partial t}(\rho\epsilon u_i) = \frac{\partial}{\partial x_j}[(\mu + \frac{\mu_t}{\sigma_\epsilon})\frac{\partial \epsilon}{\partial x_j}] + C_{1\epsilon}\frac{\epsilon}{\kappa}(P_\kappa + C_{3\epsilon}P_b) - C_{2\epsilon}\rho\frac{\epsilon^2}{\kappa} + S_\epsilon$$

Where :

- $\mu_t = \rho C_\mu \frac{\kappa^2}{\epsilon}$
- $P_\kappa = -\rho\overline{u_i' u_j'}\frac{\partial u_j}{\partial x_i}$ represents the generation of turbulence kinetic energy due to the mean velocity gradients
- P_b represents the effect of buoyancy : $P_b = \beta g_i \frac{\mu_t}{Pr_t}\frac{\partial T}{\partial x_i}$
- Y_M represents the contribution of the fluctuation dilatation in compressible turbulence to the overall dissipation rate
- S is the modulus of the mea rate-of-strain-tensor, defined as : $S \equiv \sqrt{2S_{ij}S_{ij}}$
- Other terms, $C_{1\epsilon} = 1.44$ $C_{2\epsilon} = 1,92$ $C_\mu = 0.09$ $\sigma_\kappa = 1.0$ and $\sigma_\epsilon = 1.3$ are constants that are determined empirically (These values are used in most of cases)

3.3.1.2 Realizable κ-ϵ Model

The Realizable κ-ϵ model is a more recent model different from the standard k-ϵ in two ways :

- The realizable κ-ϵ model contains a new formulation for the turbulent viscosity
- A new transport equation for the dissipation rate ϵ has also been carried out, derived from an exact equation for the transport of the mean-square vorticity fluctuation.

The term "realizable" comes from the fact that this model is more accurate with respect to some mathematical constraints, as the Reynolds stress, or the physics of turbulent flows. One of the major benefit of the realizable model is that it provides proper results for flows involving rotation. On the other side, one limitation of the realizable κ-ϵ model is that it produces non-physical turbulent viscosities when the computational domain contains both rotating and stationary fluid zones.

For turbulent kinetic energy κ :

$$\frac{\partial}{\partial t}(\rho\kappa) + \frac{\partial}{\partial t}(\rho\kappa u_j) = \frac{\partial}{\partial x_j}[(\mu + \frac{\mu_t}{\sigma_\kappa})\frac{\partial \kappa}{\partial x_j}] + P_\kappa + G_b - \rho\epsilon - Y_M + S_\kappa$$

For dissipation ϵ :

$$\frac{\partial}{\partial t}(\rho\epsilon) + \frac{\partial}{\partial t}(\rho\epsilon u_j) = \frac{\partial}{\partial x_j}[(\mu + \frac{\mu_t}{\sigma_\epsilon})\frac{\partial \epsilon}{\partial x_j}] + \rho C_1 S_\epsilon - \rho C_2 \frac{\epsilon^2}{\kappa + \sqrt{\nu\epsilon}} + C_{1\epsilon}\frac{\epsilon}{\kappa}C_{3\epsilon}P_b + S_\epsilon$$

Where :

- $C_1 = max[0.43, \frac{\eta}{\eta+5}]$
- $\eta = S\frac{\kappa}{\epsilon}$
- $S \equiv \sqrt{2S_{ij}S_{ij}}$
- μ_t is still equal to $\rho C_\mu \frac{\kappa^2}{\epsilon}$ but the main difference here is that C_μ is no longer constant. It depends then on the mean strain and rotation rates, the angular velocity of the system rotation and the turbulence fields

The κ equation is the same as in the standard $\kappa - \epsilon$ model, except that constants are different. These latter are equal to : $C_{1\epsilon} = 1.44$, $C_2 = 1.9$, $\sigma_\kappa = 1.0$ and $\sigma_\epsilon = 1.2$

Chapter 4

Airfoil theory

The blades of the turbine used in the GreenValve are NACA airfoils, whose shape will be chosen depending on the parameters that ought to be optimized. In light of these considerations, the theory behind airfoils behavior must be tackled to understand how the airfoil shape can influence the performance of the whole turbine, and what mechanisms are behind it.

Considering a fluid flowing around the surface of a body, it exerts a force on the latter, which can be divided in two parts : The lift force, which is the component of this force that is perpendicular to the oncoming flow direction, and the drag force, which is then parallel to the flow direction. In the case in which the fluid is water, the lift force is called hydrodynamic force and the drag force is fluid resistance. Yet, it is worth noticing that lift and drag forces are only generated by the interaction and contact of a solid body with a fluid. In other words, if there is no fluid, lift and drag forces can't appear. More importantly, these forces depend on the difference of velocity between the solid object and the fluid, which means there must be motion between the object and the fluid to develop these forces.

As the origin of these phenomena is very complex, particularly concerning the lift force, for which it still exists several theories to explain its cause, it won't be treated in this chapter.

The two components of the hydrodynamic force acting on the airfoil can be summed up in the following figure :

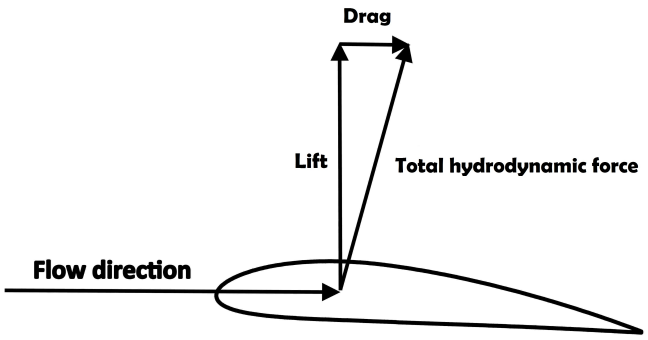

Figure 4.1: Components of the Hydrodynamic Force

4.1 Lift Forces

As it has been just said, the lift force represents the perpendicular component of the oncoming flow. The deviation of the fluid flow downward, due to the shape of the airfoil, generates an upward reaction, the lift force, as it can be observed in the figure above:

4.1.1 Formulation

The lift force (expressed in Newton) can be determined using the following equation :

$$F_L = \frac{1}{2}\rho V^2 S C_L$$

Where :

- ρ is the density of the fluid, expressed in kg/m^3
- V the relative velocity of the fluid, in m/s
- S the area of the airfoil, in m^2
- C_L is the lift coefficient (dimensionless and determined experimentally) which depends on the section shape, the angle of attack of the fluid, its Reynolds number and its Mach number.

4.2 Drag Forces

The drag force is the inertial force acting opposite to the direction of motion of a body or object, moving through a fluid.

4.2.1 Formulation

Like the lift force, the drag force depends also on the properties of the fluid and on the shape of the body. Then, it can be expressed using the following equation, very similar to the one governing the lift force :

$$F_D = \frac{1}{2}\rho V^2 S C_D$$

Where :

- ρ is the density of the fluid, expressed in kg/m^3
- V the relative velocity of the fluid, in m/s
- S the area of the airfoil, in m^2
- C_D is the drag coefficient (dimensionless number) which is an experimental coefficient depending in the section shape, the angle of attack of the fluid and on the Reynolds number

4.3 Hydrodynamic coefficients

The hydrodynamic coefficients, *i.e.* the lift and drag coefficients (Respectively noted C_d and C_l) are two important parameters that will be calculated and compared to the experimental results gathered in the literature. The fact that they're dimensionless numbers make them particularly easy to compare, from different configurations and simulations; as they already bear in mind the specificities of their geometry (Among that, the dimension of the considered airfoil) and their surrounding environment.

In consequence, for a considered airfoil profile, the evolution of the values of the hydrodynamic coefficients, as a function, for instance, of the angle of attack or the Reynolds Number, will be constant, regardless of whether a 2D or 3D problem is considered, or the fluid acting on it.

Chapter 5

Geometry

Before running any simulation, it is important to define geometrically the studied domain, either in 2D or in 3D. In fact, in this chapter will be defined the reference system used all along the followings chapter in order to give consistence to the analysis of the results obtained, in the light of their physical meaning.

5.1 General considerations

First of all, the half cylinder considered is a 80 mm diameter one. On its half length is located the turbine, composed by 3 blades which are making an angle of 120° to each other, as presented in the following figure :

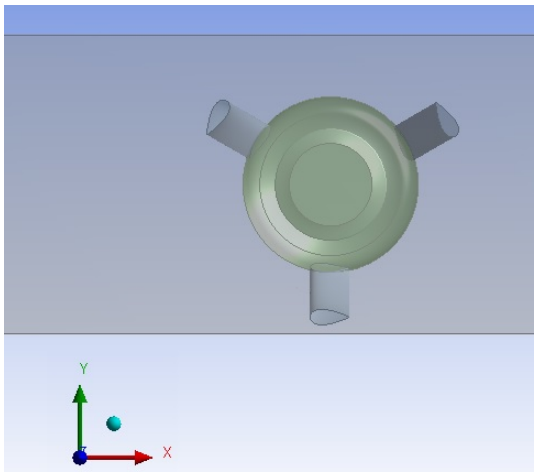

Figure 5.1: Symmetrical axis of the tube

5.2 Reference system

Its origin is set in the center of the circle that contains the three blades, and it is used to evaluate the parameters evolution for a whole rotational lap, in a range between 0° and 360°. The position of the reference center system is particularly important when calculating values of moment developed by the three blades. As the rotation physical direction of the blades is clockwise, and the reference system considered is a direct orthonormed one, it means that positive values of moment imply a counterclockwise rotation. As a matter of fact, it is worth noticing, considering the moment due to the fluid, that it has a positive effect on the rotation of the blades when its value is negative.

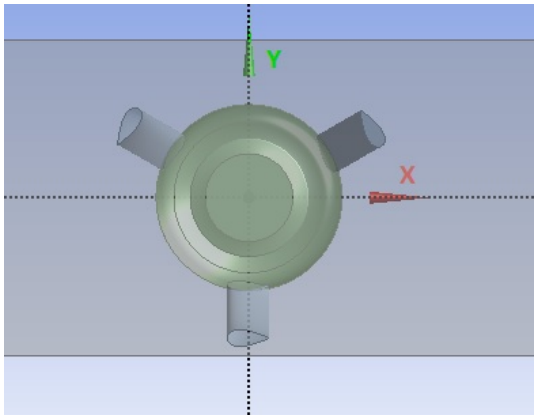

Figure 5.2: Reference system's origin

5.3 Position of the blades

Different positions of the blades have been considered in order to understand the behavior of several parameters such as flow coefficient, drag, lift and moment coefficients with reference to the angle of attack considered. The latter is defined as the angle between the reference line of the airfoil, the chord line, and the vector representing the relative motion between the body and the fluid through which it is moving. In our case, this vector is always directed along the x-direction, that is to say, the velocity is always running along the length of the tube. The following situations have been studied, for an angle of attack, noted α, equal to : 0°, 30°, 60°, 90° and are presented in the following figures.

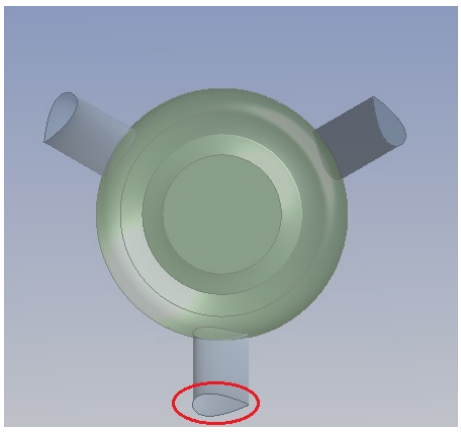

Figure 5.3: Position of the blades for $\alpha = 0^{\circ}$

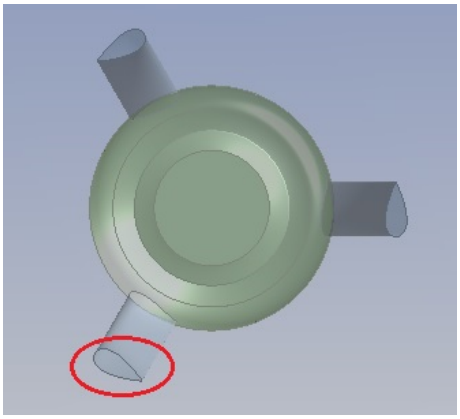

Figure 5.4: Position of the blades for $\alpha = 30^{\circ}$

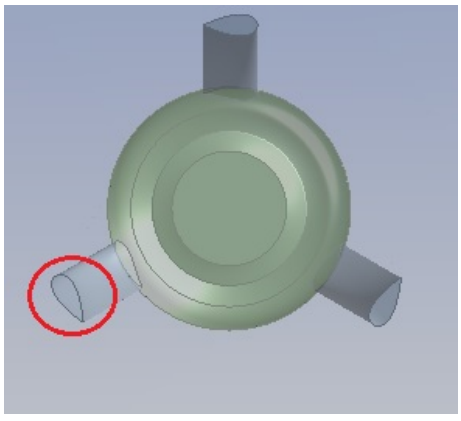

Figure 5.5: Position of the blades for $\alpha = 60^{\circ}$

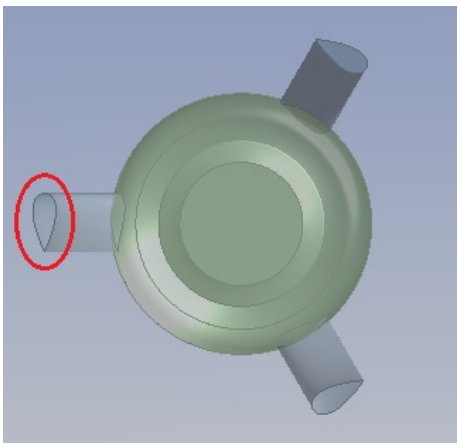

Figure 5.6: Position of the blades for $\alpha = 90^{\circ}$

Chapter 6

Setup

In this chapter will be explained the different parameters which have been employed in Fluent to run the simulations that will be presented in the following chapter.

6.1 Model

The first step is to define the model that will be used. A viscous Realizable κ-ϵ one have been considered, combined to an enhanced wall treatment, which uses a blended function to go between a two-layer model and standard wall functions. If the mesh near the wall is fine enough, the two-layer model is used. Otherwise, standard wall functions are used.

6.2 Material

An important step in the setup of the model is to define the materials and their physical properties. In our case, liquid water is running through the pipe. Properties as density and viscosity must be defined. The default values have been kept, it means that density has been chosen equal to 998,2 kg/m^3 and the viscosity equal to 0,001003 $kg/(m.s)$.

6.3 Boundary conditions

All the boundary conditions must be defined to make the difference between fluid and solid parts.
The cylinder and the turbine are considered as walls. It is used to bound fluid and solid regions The inlet fluid section must be defined. it has been chosen a fluid velocity inlet equal to $5m/s$. The outlet part, defined as a pressure-outlet one. Pressure outlet boundary conditions require the specification of a static (gauge) pressure at the outlet boundary, but only while the flow is subsonic. As the fluid is incompressible, the gauge pressure value can be set to 0.
Concerning the middle part of the tube (the yellow one in the following figure), a symmetry boundary condition must be defined, because the considered physical geometry have a

mirror symmetry. This allows to consider only a half part of the whole physical model in order to save a significant amount of computational time.

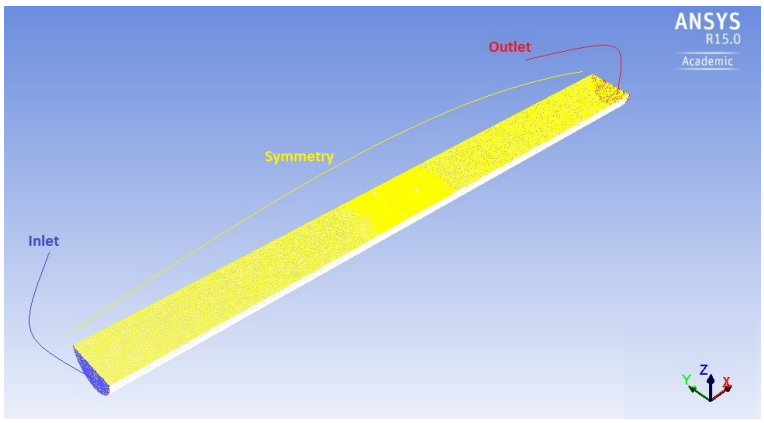

Figure 6.1: Setup

6.4 Reference values

Define reference values is an important step as these informations will be used by Fluent to calculate parameters that are not directly extracted from the simulations. For instance, once Fluent gets the force acting on a blade, reference values will be used to reach the drag and lift coefficients, as they depend on the density, the length, the area and the velocity.

They are presented in the following figure :

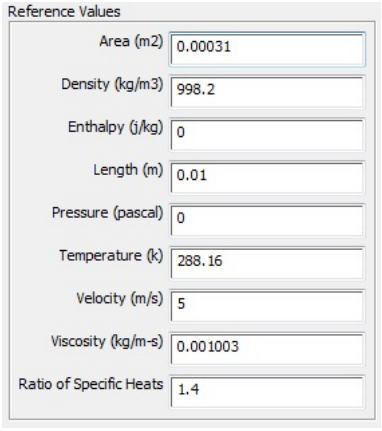

Figure 6.2: Reference values

6.5 Solver

The pressure velocity coupling method, along with the standard SIMPLE (Semi-Implicit Method for Pressure-Linked Equations) algorithm has been chosen. It is the one regularly used for RANS simulation, in particular in [7[and [16] It gives an approximation of the velocity field obtained by solving the momentum equation. The pressure gradient term is calculated using the pressure distribution from the previous iteration or an initial guess. This is an iterative algorithm.

Chapter 7

2D models

In this chapter will be developed several two dimensional models, in order to understand the influence of the particular conditions we're dealing with inside the tube. In fact, the confined and unconfined cases will be investigated, as well as the influence of blades on each other, to have a more precise idea on how these affect the behavior of the airfoil.

7.1 Introduction

The studied case has some important constraints with respect to those used in the literature. In fact, they are given results obtained under standard roughness conditions at a Reynolds number of 6 million, which is far from the conditions we're dealing with inside the tube. Then, the experimental data available lie out of our range of interest. In the case of a NACA 0040 airfoil profile, there are no available experimental data for the kind of case that we're dealing with. Moreover, concerning the mesh; even if a non confined case should be considered at the beginning, to compare with the literature, it must be taken into account in the way to mesh the grid, to anticipate cases which will be developed further.

The adopted mesh is presented in the following figure :

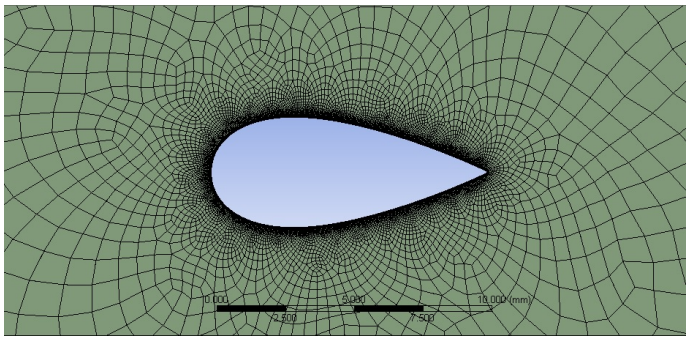

Figure 7.1: Mesh around the blade

Moreover, the thickness of the boundary layer δ, that is inversely proportional to the square root of the velocity, decreases with increasing velocity. The mesh should be therefore more refined for high Reynolds number and less refined for lower Reynolds number (in the area close to the wall boundary). For this reason it is not useful to set the mesh on the basis of a comparison with experimental data at R_e equal to 6 million.

7.2 Reynolds number

As the conditions in which have been obtained experimental results are widely different from the ones used for this project, mainly concerning its Reynolds Number, it is important to understand how this latter could affect the results on the drag and lift coefficients. To this aim, one will simulate the same model several times, changing only the value of the dynamic viscosity ν, which has a direct effect on the value of the Reynolds Number, expressed as follow :

$$R_e = \frac{UD}{\nu}$$

Where :

- R_e is the Reynolds Number
- U is the mean velocity of the object relative to the fluid, in m/s
- D the chord length of the airfoil, in m
- ρ the density of the fluid, in kg/m^3
- μ is the dynamic viscosity equal to $1,00.10^{-3} Pa.s$ for the water

For the investigated case, the mean velocity is equal to $5m/s$, the chord length of the airfoil is of $0,01m$. The fluid considered being water, its density is equal to 998 kg/m^3 and its dynamic viscosity is $1,00.10^{-3}$ Pa.s. As a consequence, the Reynolds Number is approximately equal to 50 000.

7.3 Convergence of the results

In order to get results independent from the grid, several models have been performed, with different sizes of the mesh domain. This operation has been repeated for different values of the angle of attack. It is important to note that the fluid velocity inlet has been taken equal to $5m/s$ (And it will be the case for all simulations).

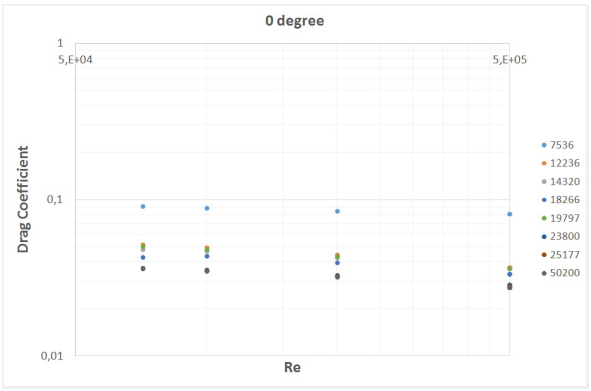

Figure 7.2: Values of Drag Coefficient with respect to the value of the Reynolds Number : Convergence of the grid for a 0 degree angle of attack

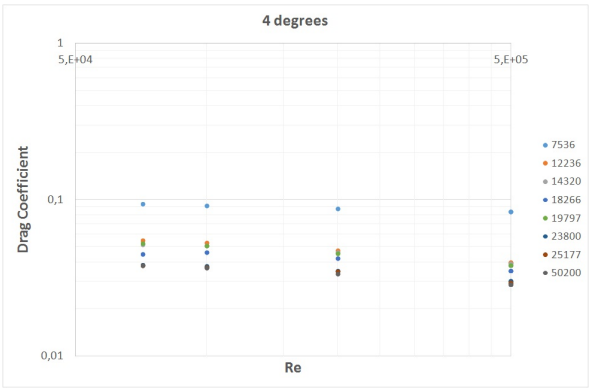

Figure 7.3: Values of Drag Coefficient with respect to the value of the Reynolds Number : Convergence of the grid for a 4 degrees angle of attack

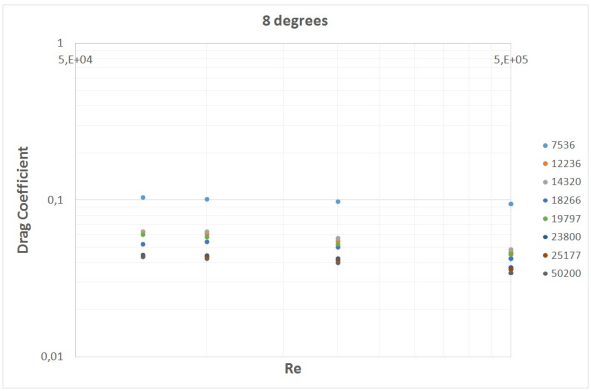

Figure 7.4: Values of Drag Coefficient with respect to the value of the Reynolds Number : Convergence of the grid for a 8 degrees angle of attack

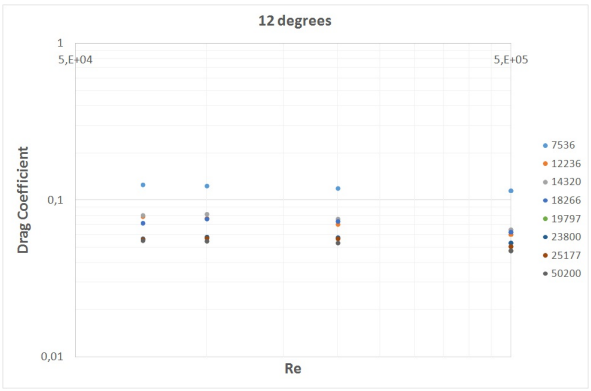

Figure 7.5: Values of Drag Coefficient with respect to the value of the Reynolds Number : Convergence of the grid for a 12 degrees angle of attack

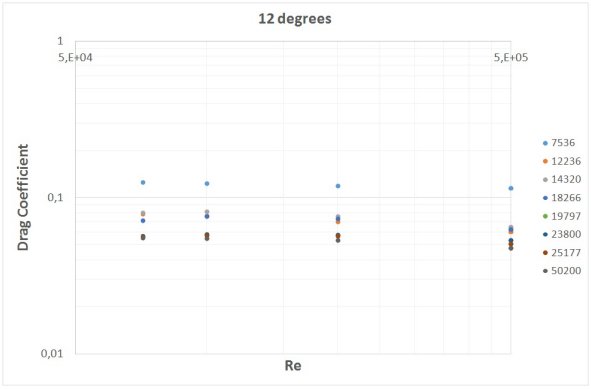

Figure 7.6: Values of Drag Coefficient with respect to the value of the Reynolds Number : Convergence of the grid for a 16 degrees angle of attack

Two remarks can be made from these figures :
The first one is that the value of the drag is increasing when the angle of attack grows. This is due to the fact that the highest is the angle of attack, the more disrupted is the flow. This will create a turbulence zone due to an airflow separation on the wing, which size depends directly to the angle of attack, and which makes the drag higher.

7.4 Confined model

As unconfined simulations have been carried, the blade will be put in the pipe to see how the confinement, and also the two other blades, affect the values of the drag and lift coefficients. In this context, one will simulate the behavior of the fluid in the case in which only one blade is present inside the tube, and others in which the whole turbine, *i.e.* 3 blades, will be put inside the tube.

For both cases, the grid size is around 90 000 meshes.

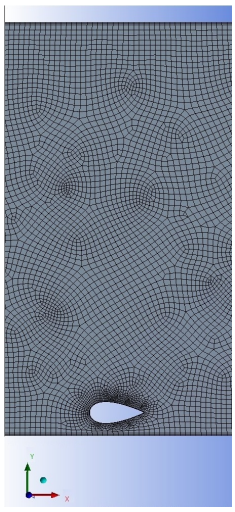

Figure 7.7: One blade into the tube

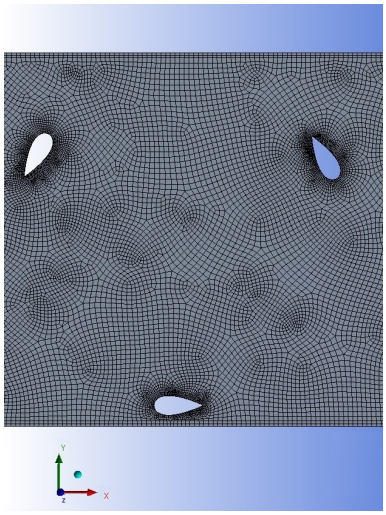

Figure 7.8: Three blades into the tube

In the considered case, the angle of attack is null when the blade is the closest to the wall. The latter will impact the values of the drag and lift coefficients. Moreover, when the three blades are considered, they will influence each other, that will impact the results.

7.4.1 Comparison for a low angle of attack

The first comparison of results has been carried out for a low angle of attack (*i.e.* $\alpha = [\![0^\circ, 16^\circ]\!]$).

Both comparison, for drag and lift coefficients, are presented in the following charts, for the three configuration cited above :

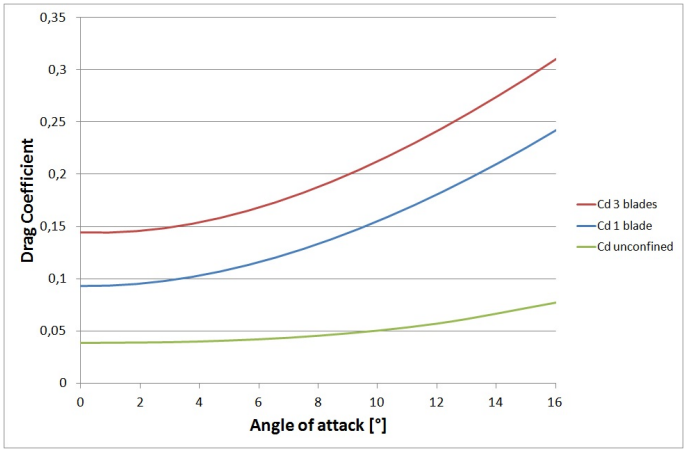

Figure 7.9: Comparison of the Drag Coefficient in 3 different configurations

From these two charts, it can be observed that the presence of walls and other blades have an increasing impact on the value of the drag coefficient, all along the considered

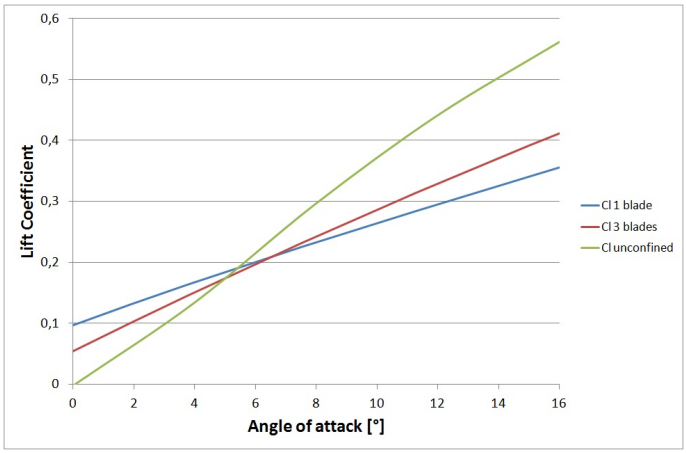

Figure 7.10: Comparison of the Lift Coefficient in 3 different configurations

interval. Yet, considering the lift coefficient, with only walls, or adding the other blades, they have a reducing influence up to $\alpha = 5^{\circ}$. Beyond this point, as the blade considered will be further to the wall, the lift coefficient in the unconfined case is higher than the two other considered cases.

On a general point of view, the increasing of the values of drag and lift coefficients can be explained as follow :

- For a low angle of attack ($\approx 0^{\circ}$)

  The influence of the airfoil on the flow path is almost negligible. This means the flow path is slightly deviated on the upper surface of the wing. Yet a turbulence appears at the end of the airfoil, and a low negative pressure can be observed, both at the extrados and at the intrados of the airfoil (However smaller at the intrados). A positive pressure is also located at the leading edge of the profile. In this case, as the negative pressure at the extrados is quite low, it makes appears a low lift force. Similarly, as the turbulence around the airfoil is weak, friction forces are reduced, then also the drag force .

- For a higher angle of attack ($\approx 15^{\circ}$)

  The flow path is significantly disrupted but the presence of the airfoil. As the flow is deviated in the upper surface of the airfoil, it makes appears a high negative pressure. On the contrary, the deviation of the flow path on the lower part of the airfoil creates a positive pressure. The differential pressure is now significant, which develops a substantial lift force. Nevertheless, the turbulence zone is also larger, that makes increase the drag force, but not as much as the lift one.

7.4.2 Comparison for a whole rotation of the turbine

The investigated range will be expanded up to 360°, in order to get a full perspective the problem and to understand how the blades have an influence on each other.

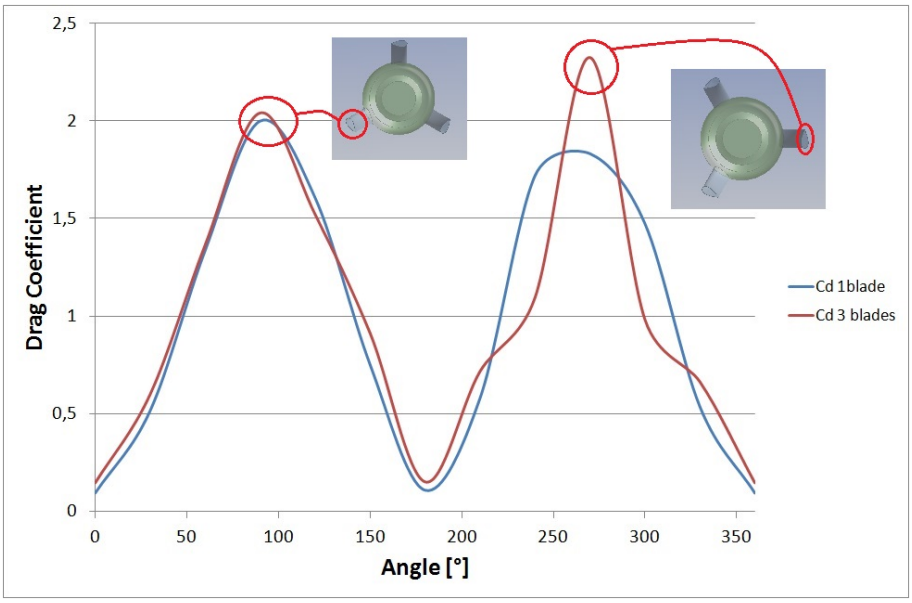

Figure 7.11: Comparison of the Drag Coefficient

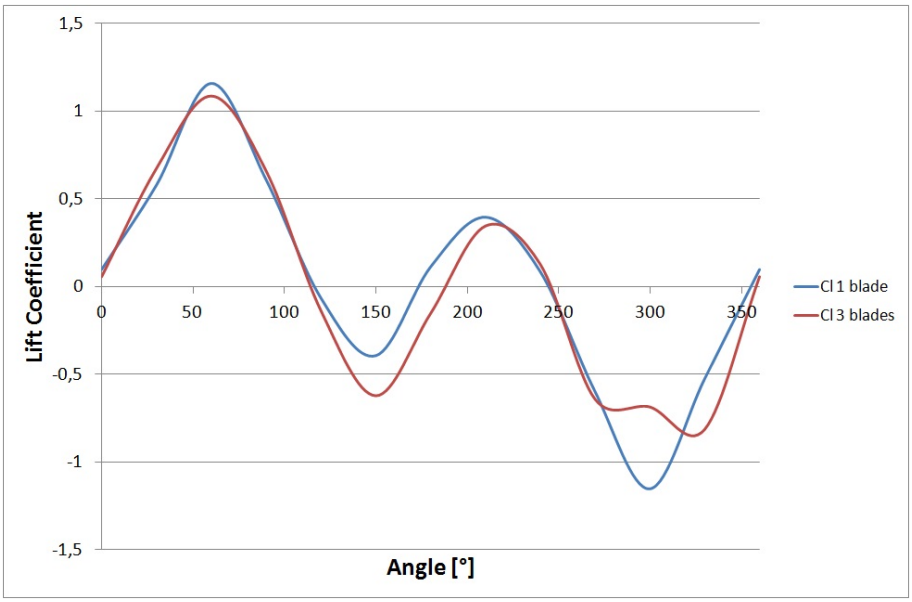

Figure 7.12: Comparison of the Lift Coefficient

Considering the whole range from 0° to 360°, one can observe that the impact of the blades on each other does not have a such significant impact on the values of drag and lift coefficients. The most important factor is probably the presence of the wall, as it can already be seen in the range $\alpha = [\![0^{\circ}, 16^{\circ}]\!]$.

7.4.3 Conclusion

It can be observed that the presence of the walls and the other blades have a increasing impact on the value of the drag coefficient, no matter the angle of attack considered. In the same way, it can be noticed that the lift coefficient is heightened in presence of other blades. As a matter of fact, as it had been explained before, Darrieus Turbine is a lift-type device, which means its draws his efficiency from the lift forces . In other words, as the confined geometry decreases values of the lift and increases those of the drag, this leads to the conclusion that this configuration implies a minor rotation of the turbine for the same input conditions.

Chapter 8

3D Models

In this chapter will be considered the three dimensional case, which corresponds to the reality of the problem we're handling. Similarly to the previous chapter, drag and lift coefficients will be obtained from fluent, as the moment developed by these forces, acting on the turbine. The fluid-structure interaction will be performed in order to quantify the mechanical constraints to which is submitted the structure, to inspect whether or not its integrity is in danger.

8.1 Introduction

A 3D model of the tube, in which the valve's body is embed will be considered now. The geometry is the same as presented before. The same way as the 2D case, drag, lift and moment coefficients will be calculated, as well as the flow coefficient, which gives informations about the valve's efficiency. Then, CFD results will be coupled to the mechanical part, through a one-way analysis, the see how the latter behavior is influenced by the presence of the fluid. Moreover, a intermediate case, called 2,5D has been performed for the purpose of making geometrical simplifications, in order to eventually save computational time.

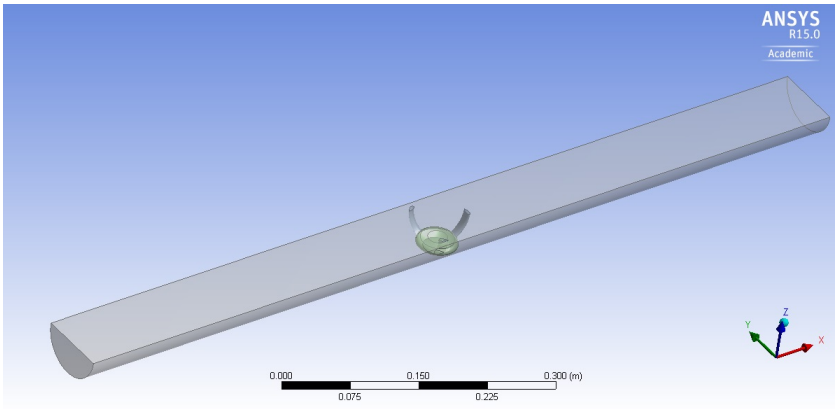

Figure 8.1: 3 dimensional tube

To make calculus faster, the problem's symmetry let us only consider a half of the structure.

8.2 Initial Position

The objectives of these simulations are diverse : First and foremost, the initial configurations of the blades will be studied. This configuration corresponds to the case presented in the following figure, and is considered as the one for which the angle of rotation of the turbine is equal to 30°.

8.2.1 Convergence of the grid

The first step will be to ensure that the size of the mesh is large enough to obtain results of lift (also known as hydrodynamic force), drag (or fluid resistance),moment and flow coefficients independent from the grid dimension. Actually, the grid number has a significant impact on the accuracy of the results. It is then necessary to create different meshes in order to use one for which results are stable. In the following charts are presented the values of each parameters discussed (drag, lift, moment and flow coefficients), and it can be concluded that the mesh becomes stable from about 3 000 000 of meshes. Of course, this value of grid number is subjective in the way that results could be slightly more accurate if the quantity of mesh would be increased, but the computational time would be significantly increased too.

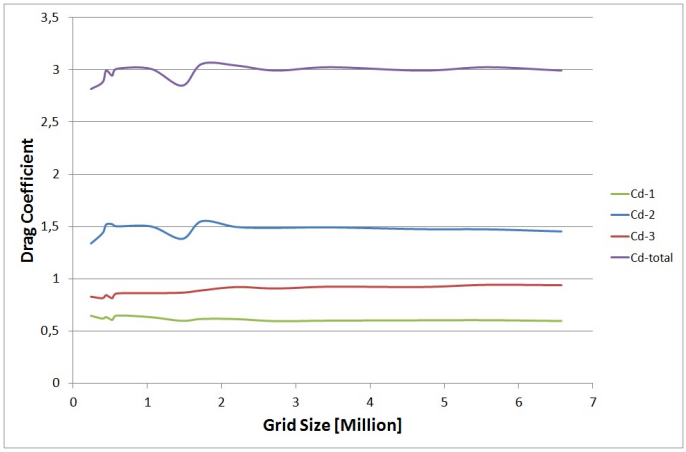

Figure 8.2: Drag Coefficient values depending on the Grid Dimension

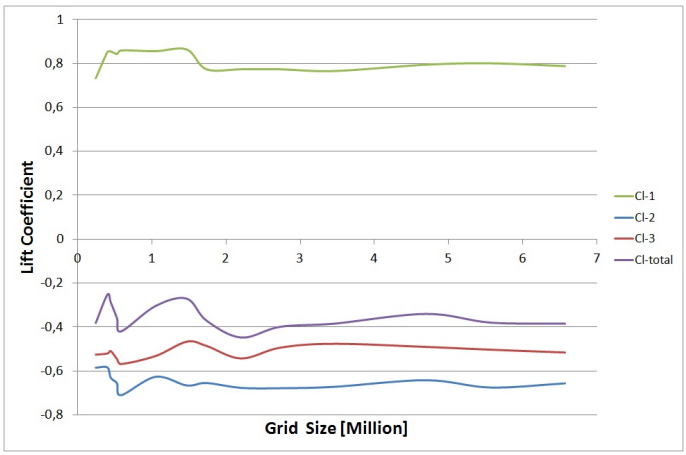

Figure 8.3: Lift Coefficient values depending on the Grid Dimension

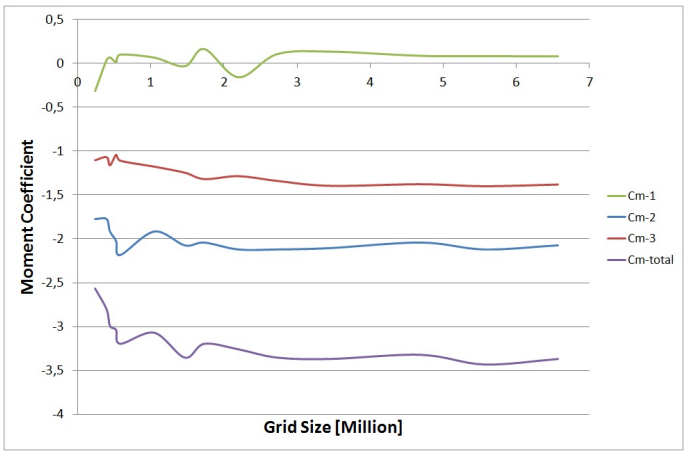

Figure 8.4: Moment Coefficient values depending on the Grid Dimension

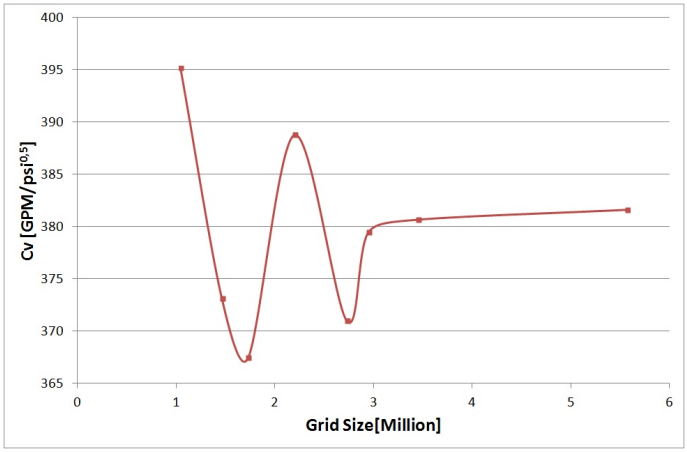

Figure 8.5: Flow coefficient values depending on the Grid Dimension

8.3 2,5D case

An intermediate case between the 2 dimensional simulation and the 3 dimensional one has been realized in order to be sure that the fluid behavior is still coherent between the several cases. In other words, all cases must have similar hydrodynamic coefficients values, as it is an dimensionless number. Only 5mm over the 40mm that compose the total half height of the tube have been considered.

The same simulations as in the two other cases have been performed in order to confront results from the simulations.

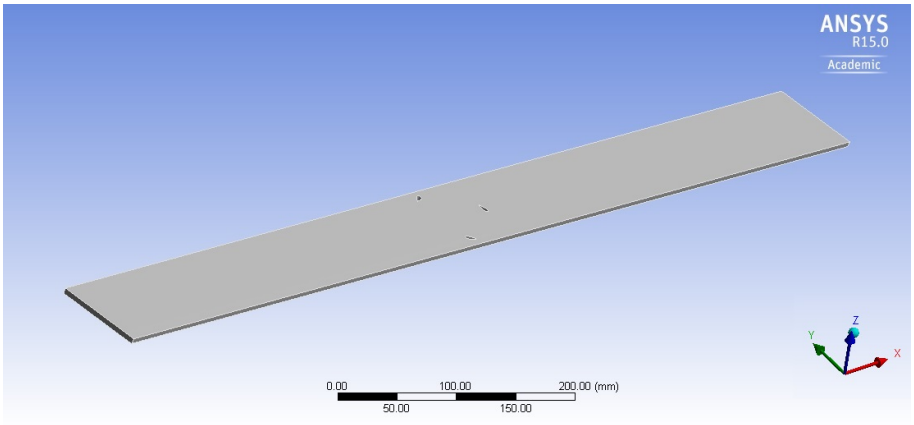

Figure 8.6: 2,5 dimensional tube

8.4 Blades positions

As this valve is made to rotate thanks to the flow passing through the tube, other positions of the blades must be tested, to understand in a more global way how the fluid impacts the valve performance, and more precisely, that of the blades. The aim will be to get values of drag, lift and moments coefficients (Respectively noted C_d, C_l and C_m) by making 30° rotations of the whole valve around the vertical axis. Obviously, as the valve is composed by 3 blades, the results of the entire rotation can be carried out modulo 120°.

In these graphics are compared the three hydrodynamics coefficients (C_d, C_l and C_m) for three different dimensional configurations. In other words, are presented the 3D, 2D and 2,5D cases corresponding to the same configurations. The goal is thus to verify that the hydrodynamic coefficients have the same evolution, no matter which portion of the total depth is considered.

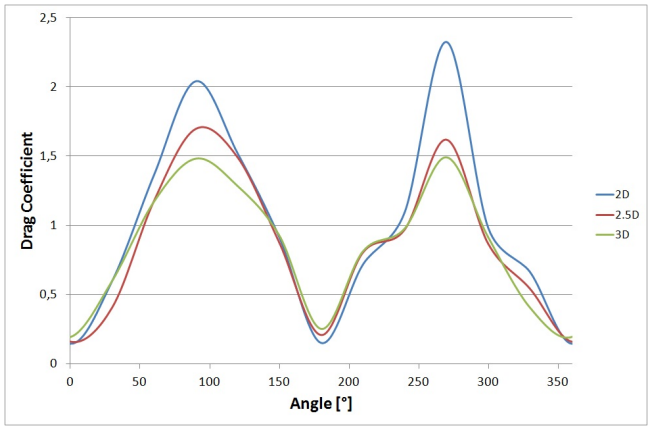

Figure 8.7: Drag Coefficient values depending on the Angle of Rotation

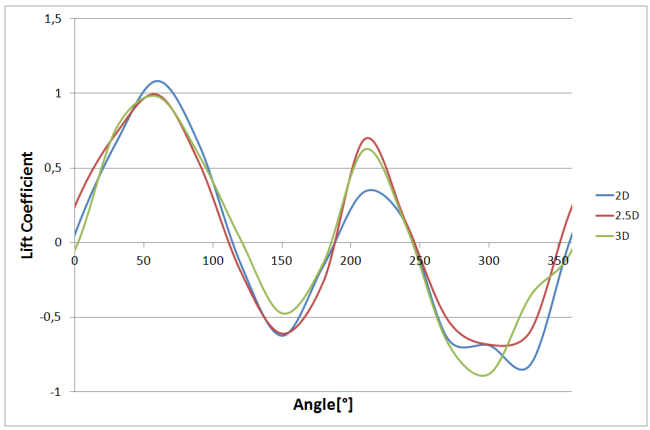

Figure 8.8: Lift Coefficient values depending on the Angle of Rotation

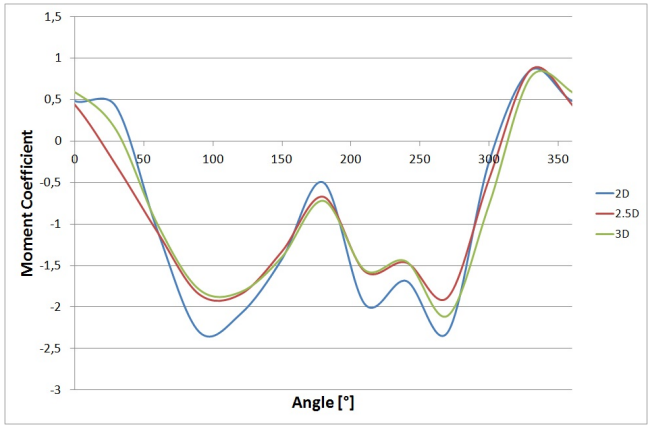

Figure 8.9: Moment Coefficient values depending on the Angle of Rotation

It can be observed that curves are quite similar to each other for every coefficient considered. Slight differences can be noticed between both 3D cases and the 2D one but they remain acceptable considering that two different dimensions are confronted. The computational calculation makes appear some differences inherent to the distinct dimensions. Concerning the moment developed by the blades, it makes the turbine spin clockwise, which corresponds to the natural, most favorable rotation of the turbine.

8.4.1 Evaluation of the C_v Parameter

In order to determine the value of the flow coefficient C_v, one has acquired values of velocity and pressure at 2 diameters upstream the GreenValve and 6 diameters downstream. The diameter of the considered tube being equal to 80 mm, values have been taken 160 mm upstream and 480 mm downstream. Once the mean velocity between the upstream and downstream points have been obtained, the flow rate can be expressed by the following formula : $Q = v_{mean}\frac{d^2}{4}\pi$ where d is the diameter of the tube. Moreover, the pressure drop Δp between the two positions can also be calculated, and then, for a specific configuration, the flow coefficient is expressed as :

$$C_v = \frac{Q}{N_1\sqrt{\frac{\Delta p}{\rho/\rho_0}}}$$

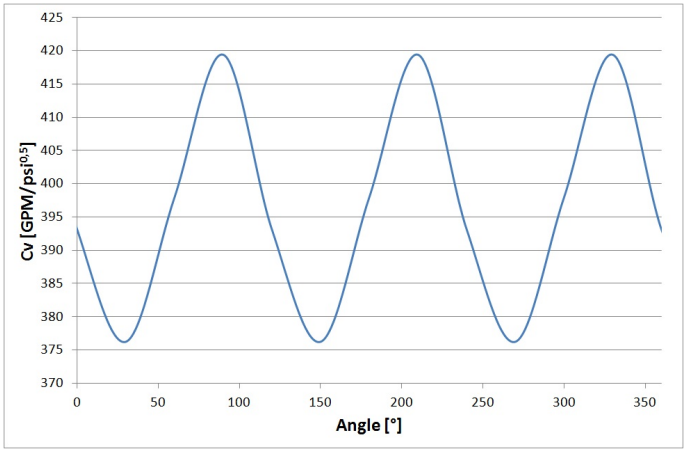

Figure 8.10: C_v values depending on the Angle of Rotation

The above chart shows the value of the flow coefficient highly depends on the position on the considered blade, which is not such a good thing, as the C_v depends directly on the pressure drop and on the flow rate. In other words, the turbine efficiency would significantly depend on the blades position. Yet, these values have been obtained in the case in which blades were fixed, and several simulations had been carried out, changing their positions. Moreover, in the case of an unsteady simulations, the turbine would rotate under the action the incoming fluid, which could create some additional interaction.

8.5 Conclusion

Once the fluid behavior have been studied, it's time to make fluid and mechanical part interact. In the following figure is presented the pressure developed by the fluid acting on the turbine's surface.

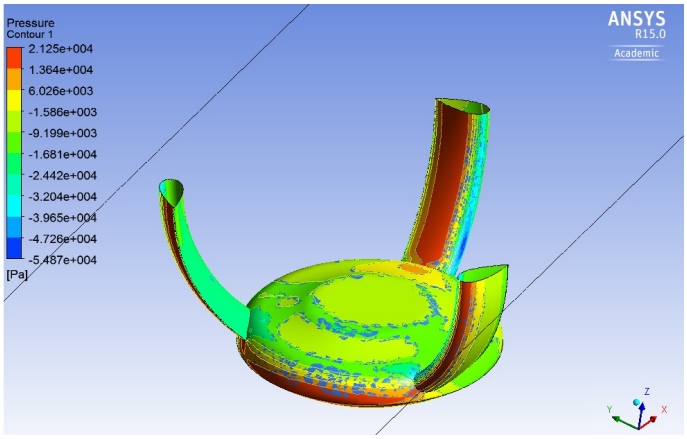

Figure 8.11: f

This pressure will be used in the structural part to define the stress field.

Chapter 9

Fluid-Structure Interaction

The main goal of the thesis is to determine whether or not the turbine can resist to stresses implied by the fluid running through the tube. To this aim, a one way fluid-structure interaction model has been performed. It means that fluid and structural simulations are solved separately but the fluid force data is transferred from the solved fluid simulation into the structural one using the physics coupling interface.

9.1 Material

The material used for the whole valve is the same as the one from the prototype used during experimental tests. It is a thermoplastic material for design Series 3D printers, from the Stratasys company, named ABSplus-P430, whose properties presented in the following page are extracted from the manufacturer's catalog :

P430 ABSplus Material Properties

A true industrial thermoplastic, ABS is widely used throughout industry. When combined with Dimension 3D printers it becomes the ideal solution to printing 3D models in an office environment.

MECHANICAL PROPERTIES[1]

	Test Method	Imperial	Metric
Tensile Strength, Type 1, 2 in/min (51 mm/min) 0.125	ASTM D638	5,300 psi	37 MPa
Tensile Modulus, Type 1, 2 in/min (51 mm/min) 0.125	ASTM D638	330,000 psi	2,320 MPa
Tensile Elongation, Type 1, 2 in/min (51 mm/min) 0.125	ASTM D638	3%	3%
Flexural Delamination	ASTM D790	4,500 psi	31 MPa
Flexural Strength	ASTM D790	7,600 psi	53 MPa
Flexural Modulus	ASTM D790	320,000 psi	2250 MPa
IZOD Impact, notched, (Method A, 73° (23° C))	ASTM D256	2.0 ft-lb/in	106 J/m

THERMAL PROPERTIES[3]

	Test Method	Imperial	Metric
Heat Deflection (HDT) @ 66 psi (0.5 MPa)	ASTM D648	204° F	96° C
Heat Deflection (HDT) @ 264 psi (1.8 MPa)	ASTM D648	180° F	82° C
Glass Transition (TG)	DMA (SSYS)	226° F	108° C
Melt Point		(NA)[2]	(NA)[2]

OTHER[3]

	Test Method	Value
Specific Gravity	ASTM D792	1.04
Vertical Burning Test	UL94	HB
Coefficient of Thermal Expansion	ASTM E831	4.90E-05 in/in/F
Dielectric Strength (kV / mm)	IEC 60112	28.0

[1] Build orientation is on side edge except for flexural delamination which is upright.

[2] Not applicable (NA) due to amorphous nature. Material does not display a melting point.

[3] Literature value unless otherwise noted.

APPEARANCE

Standard colors include natural, black, dark gray red, blue, nectarine (orange), florescent yellow and olive green.

SYSTEM AVAILABILITY

Dimension Elite
Dimension BST 1200es
Dimension SST 1200es

Dimension Printing, a business unit
of Stratasys, Inc.
7665 Commerce Way
Eden Prairie, MN 55344-2080 U.S.A.
866.721.9244 US Toll Free
+1.952.937.3000
info@dimensionprinting.com
www.dimensionprinting.com

In the following is presented the geometry of the considered turbine, in which the pressure due to the fluid, acting on the three blades and the base of the turbine, will be applied to the structural part in order to determine value of stress, strain and deformation experienced by this latter.

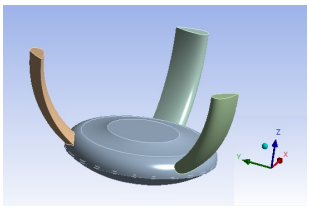

Figure 9.1: View of the turbine

Regarding the boundary conditions, a frictionless support has been imposed in the upper part of each blade, in order to take into account the symmetry of the problem. In addition, the lower part of the base has been fixed.

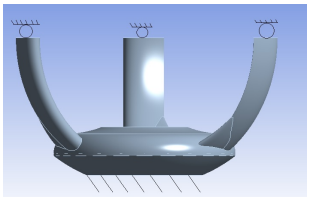

Figure 9.2: Boundary conditions on the structure

9.2 Correspondence between the CFD and mechanical

Different meshes between CFD and the mechanical part can lead to some mapping interpolation in the transfer of data, that is why these values could differ a bit. In fact, if the mesh is too coarse, the mapping interpolation will not be accurate and these values will be very far from each other, which will lead to inaccurate results.
Differences between pressure in CFD and in mechanical are stated in the following table :

CFD	Mechanical
Using contours : Shows both negative and positive gauge pressure	Using vectors : All gauges pressure are positive. It gives only magnitude, but these vectors have an orientation

Table 9.1: Difference between CFD and Mechanical

9.3 Von Mises criterion

As Infinitesimal strain hypothesis is considered, the Von Mises yield criterion can be applied. It predicts that yielding will occur wherever the distortion energy in a unit volume equals the distortion energy in the same volume when uniaxially stressed to the yield strength. Its advantage is that it allows any three-dimensional stress state to be represented as a single positive stress value. Equivalent stress is part of the maximum equivalent stress failure theory used to predict yielding in a ductile material.

Equivalent stress is related to the principal stresses by the equation :

$$\sigma_e = \frac{1}{\sqrt{2}}\sqrt{(\sigma_1 - \sigma_2)^2 + (\sigma_2 - \sigma_3)^2 + (\sigma_1 - \sigma_3)^2}$$

The Von Mises or equivalent strain ϵ_e is computed as :

$$\epsilon_e = \frac{1}{1+\nu}\sqrt{\frac{1}{2}[(\epsilon_1 - \epsilon_2)^2 + (\epsilon_2 - \epsilon_3)^2 + (\epsilon_1 - \epsilon_3)^2]}$$

9.4 Deformation

The total deformation of each part that composes the structure is also inspected.
It is obtained through to the Euclidean norm of each component deformations U_x, U_y and U_z, as :

$$U = \sqrt{U_x^2 + U_y^2 + U_z^2}$$

In the following are presented the several components of the deformation, for a parallelepipedic body.

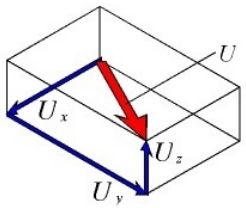

Figure 9.3: Deformation calculation

Where :

- Component deformation (Directional deformation)
- Deformed shape (Total deformation vector)

9.5 Results

In the following table are presented the results obtained for several positions of the blades, from 0° to 360° considering a 30° step.
It will give us information about the most unfavorable, damaging positions for each parameter considered.

Angle	Equivalent (Von Mises) Stress [MPa]		Equivalent Elastic Strain [-]		Total Deformation [mm]	
[°]	Min	Max	Min	Max	Min	Max
0	0,0017	1,1786	9,42E-7	0,0005	0,0001	0,0047
30	0,007	0,9607	4,07E-7	0,0004	0,0002	0,0078
60	0,0032	2,2790	2,08E-6	0,0010	0,0002	0,0121
90	0,0056	3,0811	2,53E-6	0,0013	0,0005	0,0154
120	0,0004	2,6382	1,66E-7	0,0011	0,0005	0,0139
150	0,0110	1,7233	4,83E-6	0,0007	0,0004	0,0123
180	0,0080	1,5668	3,72E-6	0,0007	0,0003	0,0069
210	0,0114	5,5421	4,93E-6	0,0025	0,0004	0,0238
240	0,0205	4,8867	9,04E-6	0,0022	0,0003	0,0214
270	0,0108	5,6285	5,29E-6	0,0025	0,0005	0,0239
300	0,0059	4,7017	2,54E-6	0,0020	0,0003	0,0150
330	0,0025	1,7366	1,12E-6	0,0008	0,0002	0,0098
360	0,0007	1,1786	9,42E-7	0,0005	0,0001	0,0047

Table 9.2: Mechanical constraints with respect to the angle of attack for a fully opened valve

In the following screen, one can observe the distribution of the velocity magnitude in the valve in the most unfavorable condition (*i.e.* $\alpha = 270°$) :

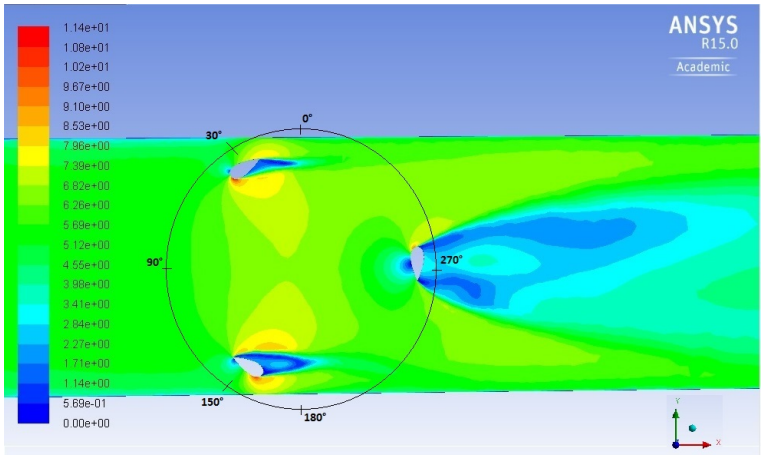

Figure 9.4: Velocity inside the tube for a fully opened valve

Several statements can be made from the above table : First of all, all the parameters (Von Mises Stress, Equivalent Elastic Strain and deformation) reach their maximum for the same configuration of the airfoil, that is to say an angle of attack equal to 270°. More generally, in the range between 210° and 300°, the airfoil is subjected to a more important stress distribution. Even if these values won't damage the turbine, it represents the most

dangerous disposition of the blades, in which the trailing edge of the airfoil is facing the fluid coming through the tube. About the deformation undergone by the structure, it is important that its maximum be minor than the distance between the blade and the pipe. Otherwise, it would probably imply massive damage for the whole structure.
Considering all the possible blades positions, the minimum distance between this latter and the pipe is of 2,35mm. For the current case, the maximum deformation value is equal to 0,024mm.

The following three charts represent the evolution of, respectively, the Von Mises Stress, the Equivalent Elastic Strain (also called Von Mises Strain) and the deformation. These values are directly taken from the previous table, and it can be observed that each one among them have the same trend.

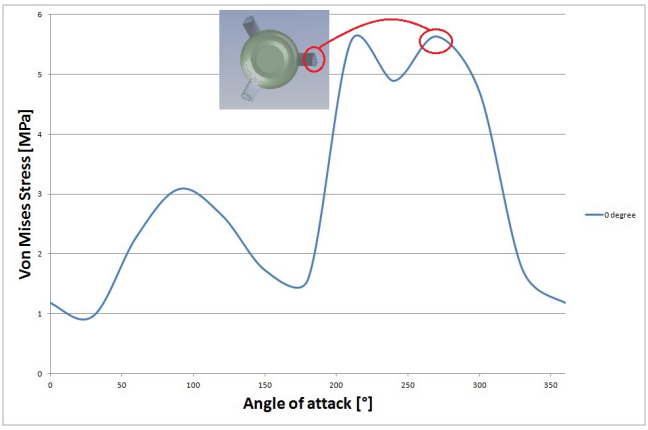

Figure 9.5: Von Mises stress with respect to the angle of attack

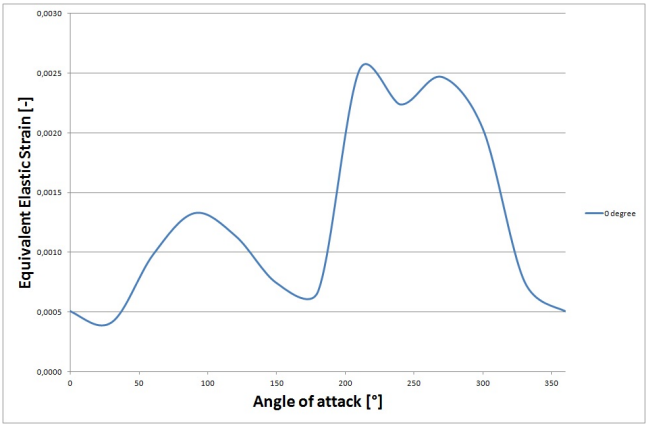

Figure 9.6: Von Mises strain with respect to the angle of attack

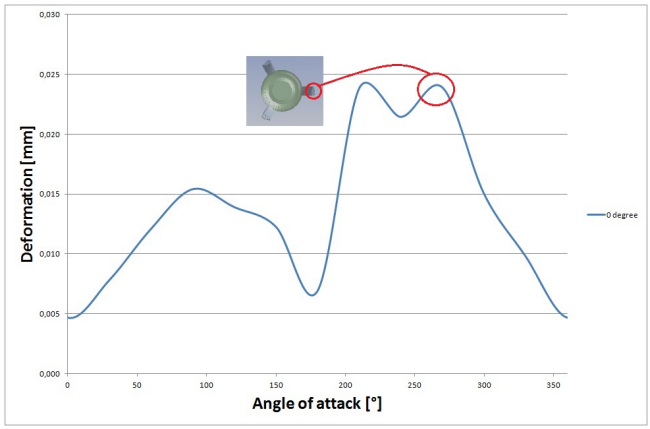

Figure 9.7: Deformation with respect to the angle of attack

9.6 Location of the maximum stresses

Once the worst position of the blade has been detected, it is worthy to know in which part of it is located the maximum values of the three parameters considered.

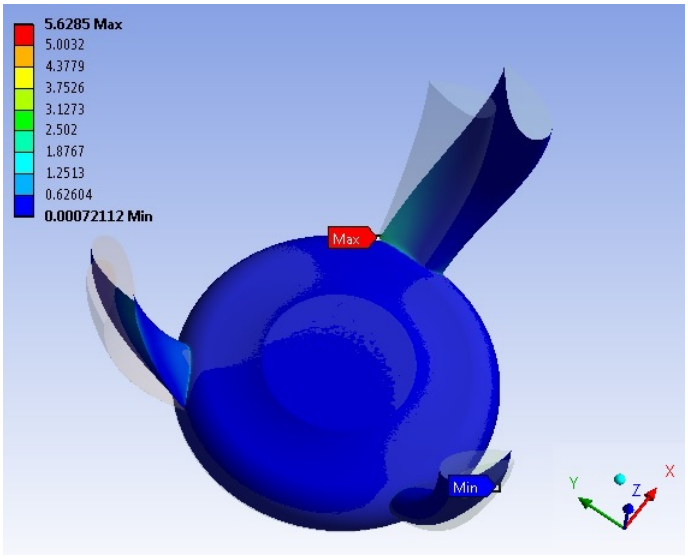

Figure 9.8: Von Mises Stress for the initial position (in MPa)

Concerning the maximum value of the Von Mises stress, it always takes place at the contact between the blade and the turbine base, no matter the position of the blade considered.

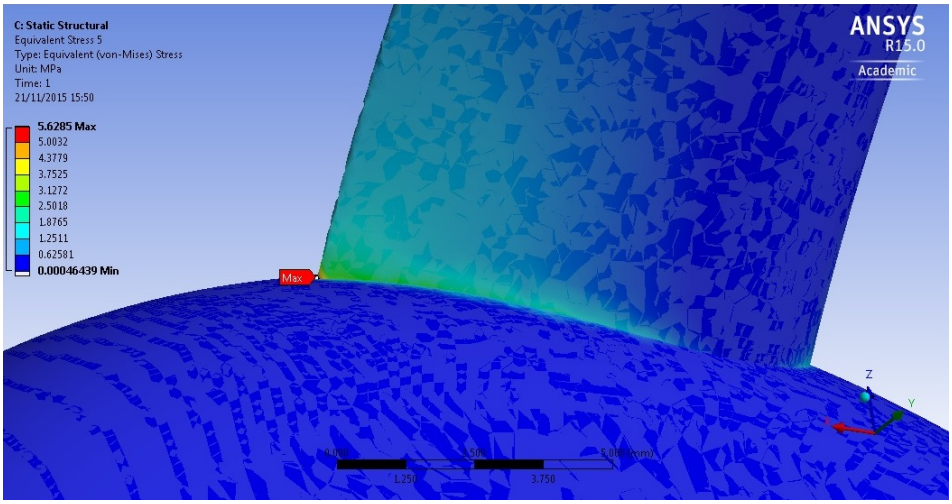

Figure 9.9: Zoom on the maximum stress location

As the maximum stress acting on the blades is equal to 5,62 MPa, which is widely smaller than the ultimate tensile strength (or yielding point), equal to 37 MPa, the material has an elastic behavior, which means deformations are completely recoverable upon removal of the load.

Now, regarding the deformation, its maximum is located in the middle of the blade. In fact, the farther we are from base, the higher is the deformation, as it can be noticed in the following :

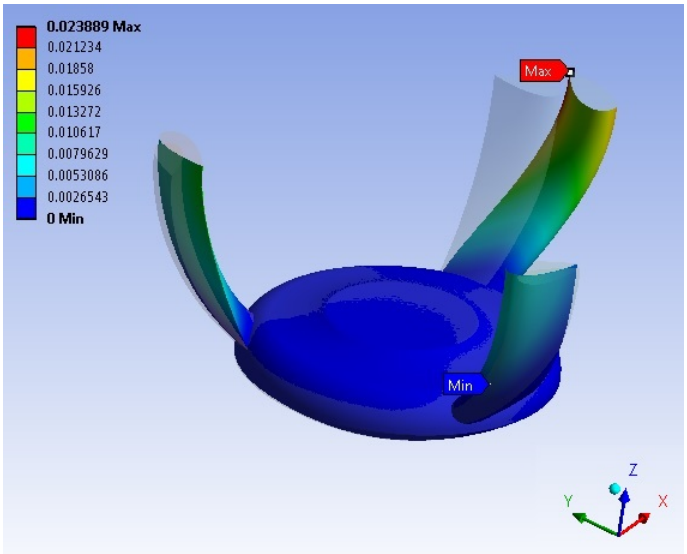

Figure 9.10: Deformation for the initial position(in mm)

Finally, when the valve is fully opened, the mechanical constraints are largely smaller than those the material limits, which is highly encouraging for the following part, in which the valve will be progressively closed, which should increase the velocity of the fluid in certain areas of the valve. Consequently, this should give rise to a more significant stress field in some specific parts of the valve.

Chapter 10

Valve closure

The GreenValve has two different functions : Controlling conditions such as flow, or pressure passing through the valve, varying its aperture, and also to recover energy dissipated by fluids. Even if it works as an On/Off valve, the transitions between the two available positions must be considered. In fact, it seems clear that the valve closure has a significant impact on the fluid's behavior, and then on the stress experienced by the the whole turbine. The impact of the valve closure ought to be quantified to understand how this action can influence the structural behavior of the turbine.

10.1 Various angles of valve closure

Several valve apertures have been considered to understand how the fluid is deviated when closing it. This will have a significant impact on the velocity of the fluid passing through the valve; there is also a massive influence on the stress field experienced by the turbine. As the configuration of the fully opened valve has already been studied in the previous section, one will be interested in three other positions, when the closure of the valve is of 30°, 45° and 60°.

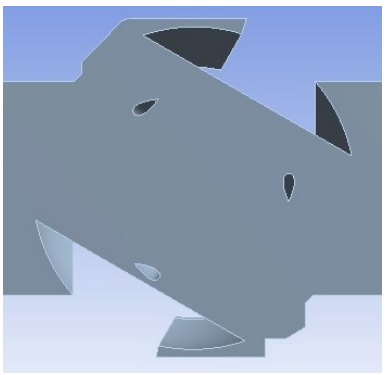

Figure 10.1: Valve closure angle $\gamma = 30^{\circ}$

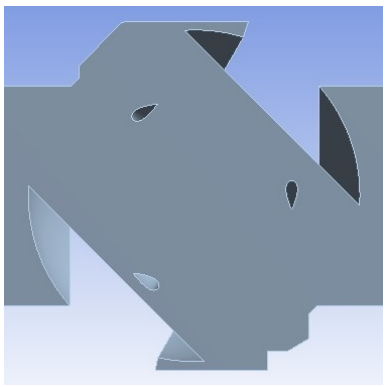

Figure 10.2: Valve closure angle $\gamma = 45^{\circ}$

These three positions will give us a good idea of the global behavior that encounters the turbine subjected to the variation of its surrounding geometry. Moreover, the valve closing

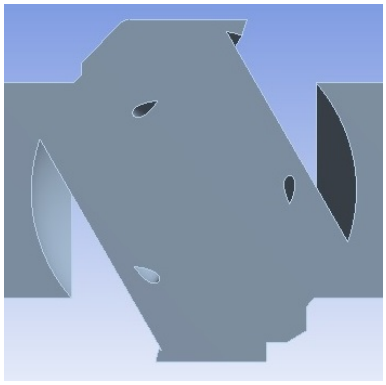

Figure 10.3: Valve closure angle $\gamma = 60^{\circ}$

has been chosen in this direction because, as it has been previously seen, the weakest part of the turbine is located at the trailing edge of the blade. Then, when the valve is closing, this part of the structure won't be subjected to an increasing load acting on it.

10.1.1 Closure angle: 30°

Considering now that the valve has a closure angle of 30°, this implies that the fluid path will be deviated compared to the case in which the valve is fully opened. In the following figure is presented the fluid path for whatsoever position of the blades. It can be noticed that the fluid velocity is almost null in some part of the valve, due to the closure of this latter. In particular, blades will be subjected to a low fluid velocity for a range between $\alpha \approx]100^{\circ};220^{\circ}[$.

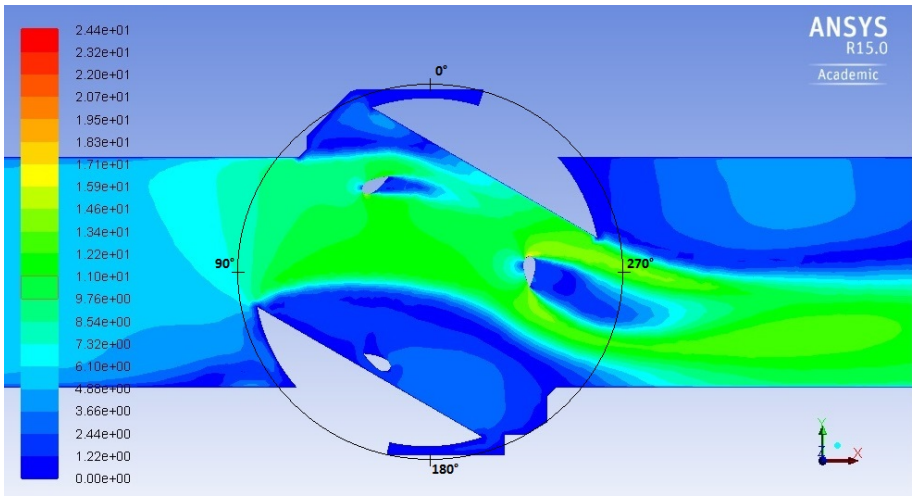

Figure 10.4: Velocity inside the tube, focusing on the valve. Closure : 30°

The low flow velocity acting on the blades has a direct impact on the three structural parameters inspected, namely the Von Mises Stress, the Elastic Strain, and the deformation

of the structure.

In fact, it can be observed in the following chart and in the corresponding graph, that the parameters noted above have low values in the range $\alpha \approx]100^{\circ};220^{\circ}[$, that is to say, where the flow velocity is significantly lower than the other parts.

Moreover, as the flow rate must be constant all along the tube, it has the effect of increasing the velocity in these other parts of the valve, corresponding to an angle of attack for the blade of $\alpha \approx]0^{\circ};100^{\circ}] \cup [220^{\circ};360^{\circ}]$.

Angle	Equivalent (Von Mises) Stress [MPa]		Equivalent Elastic Strain [-]		Total Deformation [mm]	
[°]	Min	Max	Min	Max	Min	Max
0	0,0084	1,6785	3,72E-6	0,0007	0,0028	0,0087
30	0,0014	1,9092	9,02E-7	0,0010	0,0003	0,0119
60	0,0138	3,7721	7,75E-6	0,0019	0,0004	0,0343
90	0,0108	5,9665	4,85E-6	0,0028	0,0010	0,0441
120	0,0002	0,1626	1,72E-7	8,1E-5	0,0002	0,0022
150	0,0003	0,2354	1,95E-7	0,0001	0,0004	0,0020
180	0,0002	0,3076	8,17E-8	0,0001	0,0003	0,0019
210	0,0004	0,3594	2,21E-7	0,0002	0,0004	0,0035
240	0,0040	1,5653	1,71E-6	0,0008	0,0003	0,0063
270	0,0352	13,75	1,68E-5	0,0066	0,0014	0,0720
300	0,0037	3,6069	1,61E-6	0,0016	0,0009	0,0277
330	0,0108	4,5160	4,84E-6	0,0023	0,0007	0,0337
360	0,0084	1,6785	3,72E-6	0,0007	0,0028	0,0087

Table 10.1: Mechanical constraints with respect to the angle of attack for a 30° closed valve

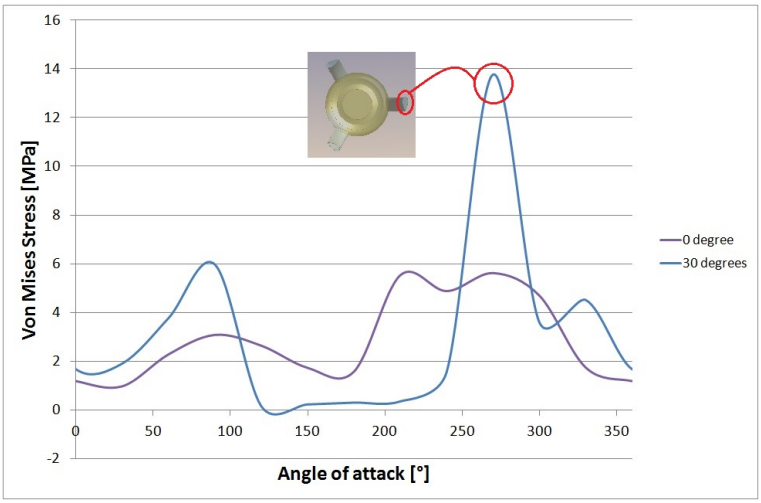

Figure 10.5: Von Mises stress with respect to the angle of attack for a 30° closed valve

The above graph compares values of the Von Mises Stress with respect to the whole range of angle of attack, for to 2 cases of valve closure; namely, a fully opened valve and a 30° closed one. One can noticed that in the range $\alpha \approx]100^{\circ};220^{\circ}[$, the stress is almost null when the valve is closed by 30°, and lower than the stress value of the fully opened valve.

In the other way, in the areas where the flow velocity has increased when the valve is part closed, the stress is increasing in a similar way.

10.1.2 Closure angle: 45°

In this case, as the valve closure is 15° more important than in the previous case, effects on the fluid velocity will be more critical. It means that a larger area of the valve will have a low fluid velocity, which, as a consequence, will give birth to a smaller path of the fluid going through the valve. As the flow rate needs to remain constant, the flow velocity will significantly increase in some parts of the valve, as it is noticeable in the following :

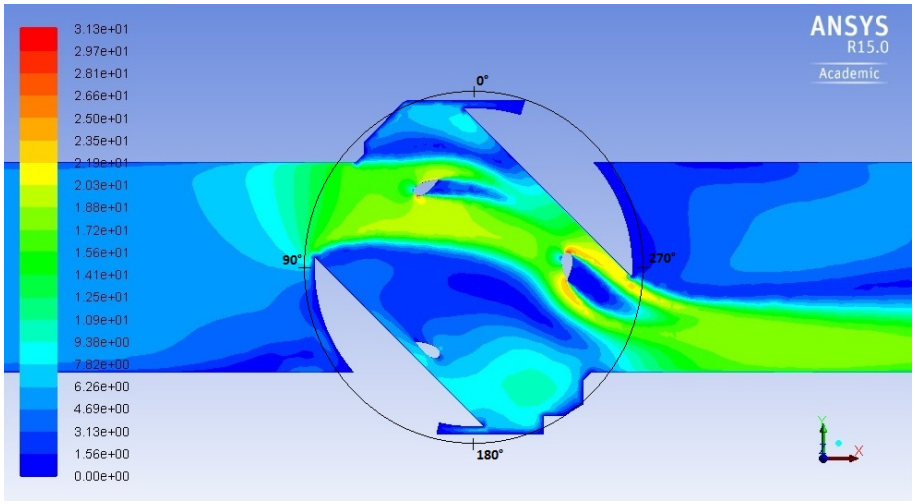

Figure 10.6: Velocity inside the tube, focusing on the valve. Closure : 45°

Angle	Equivalent (Von Mises) Stress [MPa]		Equivalent Elastic Strain [-]		Total Deformation [mm]	
[°]	Min	Max	Min	Max	Min	Max
0	0,0005	1,1387	2,29E-7	0,0005	0,0018	0,0185
30	0,0057	4,4559	2,48E-6	0,0021	0,0014	0,0405
60	0,0153	10,8630	8,45E-6	0,0051	0,0015	0,1041
90	0,0018	0,7841	8,06E-7	0,0004	0,0004	0,0050
120	0,0019	0,9946	1,32E-6	0,0005	0,0004	0,0068
150	0,0016	0,4123	7,16E-7	0,0002	0,0010	0,0022
180	0,0005	0,3132	2,26E-7	0,0002	0,0004	0,0053
210	0,0054	2,1608	2,5E-6	0,0010	0,0004	0,0182
240	0,0038	2,0284	2,2E-6	0,0010	0,0007	0,0085
270	0,0167	19,9490	8,22E-6	0,0093	0,0023	0,1006
300	0,0175	14,8760	7,92E-6	0,0069	0,0005	0,0919
330	0,0028	8,1222	1,73E-6	0,0038	0,0011	0,0480
360	0,0005	1,1387	2,29E-7	0,0005	0,0018	0,0185

Table 10.2: Mechanical constraints with respect to the angle of attack for a 45° closed valve

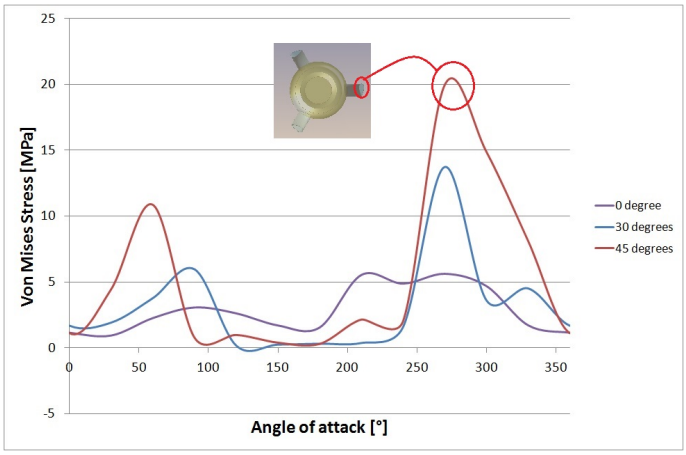

Figure 10.7: Von Mises stress with respect to the angle of attack for a 45° closed valve

Once again, it can be observed that structural parameters will be close to 0 in a wider part of the angular range, which is not located along the path followed by the fluid running through the valve. The stress will be more concentrated along the fluid path.

10.1.3 Closure angle: 60°

The closure angle will now be taken of 60°. As the valve aperture is still diminishing, the fluid velocity will be concentrated in a smaller area of the inside valve, which, as a consequence, will have a more important impact on the turbine structural behavior (and mostly on the blades that compose it) of the considered area.

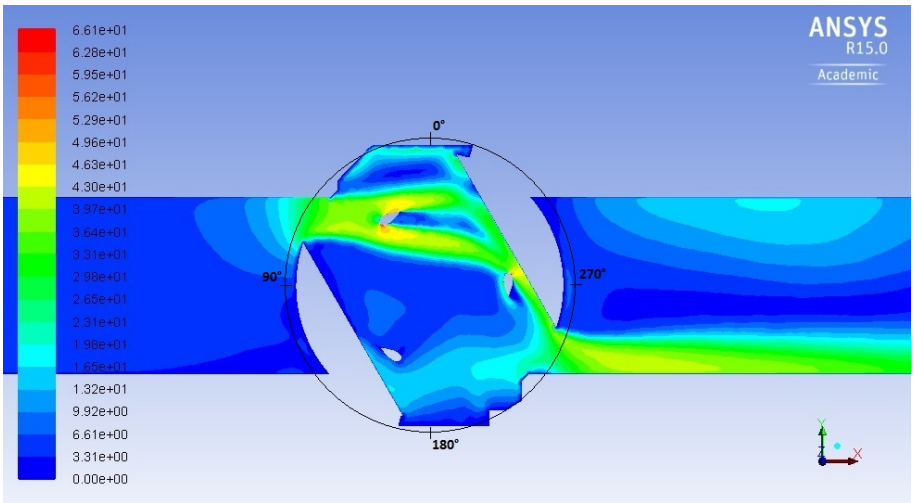

Figure 10.8: Velocity inside the tube, focusing on the valve. Rotation sphere : 60°

Angle	Equivalent (Von Mises) Stress [MPa]		Equivalent Elastic Strain [-]		Total Deformation [mm]	
[°]	Min	Max	Min	Max	Min	Max
0	0,0292	7,4744	1,4E-5	0,0037	0,0036	0,0640
30	0,0755	11	4,96E-5	0,0052	0,0063	0,2232
60	0,0155	9,5974	6,95E-6	0,0044	0,0021	0,0924
90	0,0144	4,3561	6,45E-6	0,0021	0,0030	0,0441
120	0,0153	3,2883	6,76E-6	0,0017	0,0025	0,0402
150	0,0040	1,2991	1,97E-6	0,0006	0,0030	0,0076
180	0,0105	2,6268	8,71E-6	0,0012	0,0031	0,0600
210	0,0450	6,5132	1,94E-5	0,0030	0,0041	0,1177
240	0,1066	11,9840	4,75E-5	0,0059	0,0015	0,0733
270	0,0608	25,9680	3,04E-5	0,0119	0,0036	0,1959
300	0,2289	44,4730	1,23E-4	0,0213	0,0075	0,4692
330	0,1430	13,3580	6,51E-5	0,0061	0,0027	0,0994
360	0,0292	7,4744	1,4E-5	0,0037	0,0036	0,0640

Table 10.3: Mechanical constraints with respect to the angle of attack for a 60° closed valve

It's important to remark that the position of the valve for which the maximum stress value is obtained in this ultimate case is slightly different to those in the previous cases. In fact, when the valve closure is of 60°, the maximum stress value is obtained for an angle of attack of 300° whereas it was equal to 270° for the other cases. It means that the progressive concentration of the flow path implies also, from a certain point, a modification of the most unfavorable position for the blades.

It is also worth noticing that the maximum value of the Von Mises Stress isn't located in the trailing edge anymore, but in the leading edge, which is directly subjected to the incoming fluid. Because of its physical nature, it makes this part probably stronger than the traiing edge.

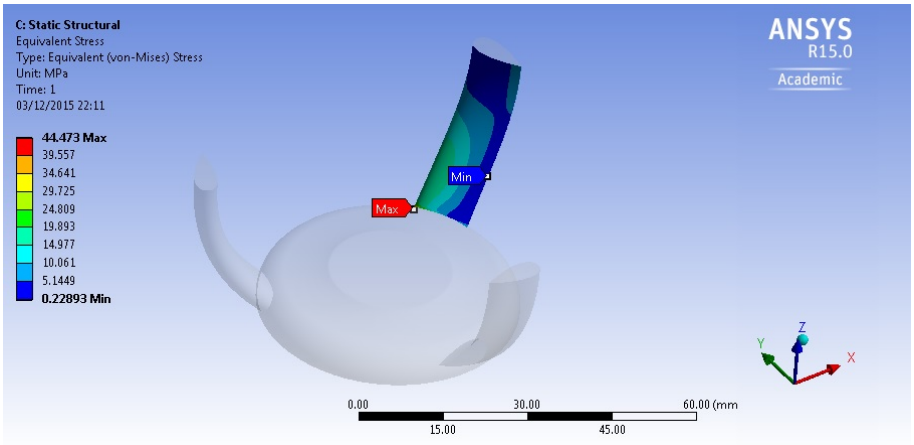

Figure 10.9: Maximum Von Mises stress location

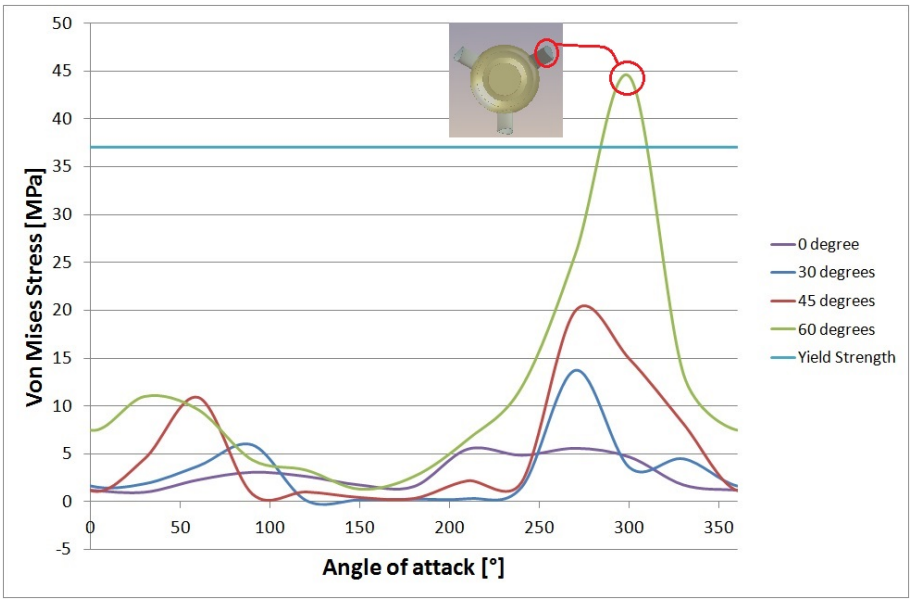

Figure 10.10: Von Mises stress with respect to the angle of attack for a 60° closed valve

Finally, as it can be shown in the previous graph, the progressive valve closure has the effect to concentrate the fluid path in a smaller area, increasing its velocity and then the mechanical stress acting on the blades that lie on its path. The maximum Von Mises stress value appears for an angle of attack α=300° and worths 44,47 MPa.

Considering the thermoplastic material used to design the turbine; Its tensural strength is equal to 37 MPa, which means that mechanic loads acting on the turbine damage it. At this point, the material has started yielding (when its Von Mises stress reaches the value of the tensural strength) and some irreversible deformations should have appeared.

Moreover, this maximum value of the Von Mises stress would probably increase again when the valve closure increases as well.

10.2 Deformations

In this section are presented the blades deformations for all considered valve closure positions.

It is an important parameter to take care of, because if the deformations is too high, one of the blade (probably the nearest one to the wall, *i.e.* for α equal to 0° or 180°) could touch the pipe, which could compromise the integrity of the whole structural system.

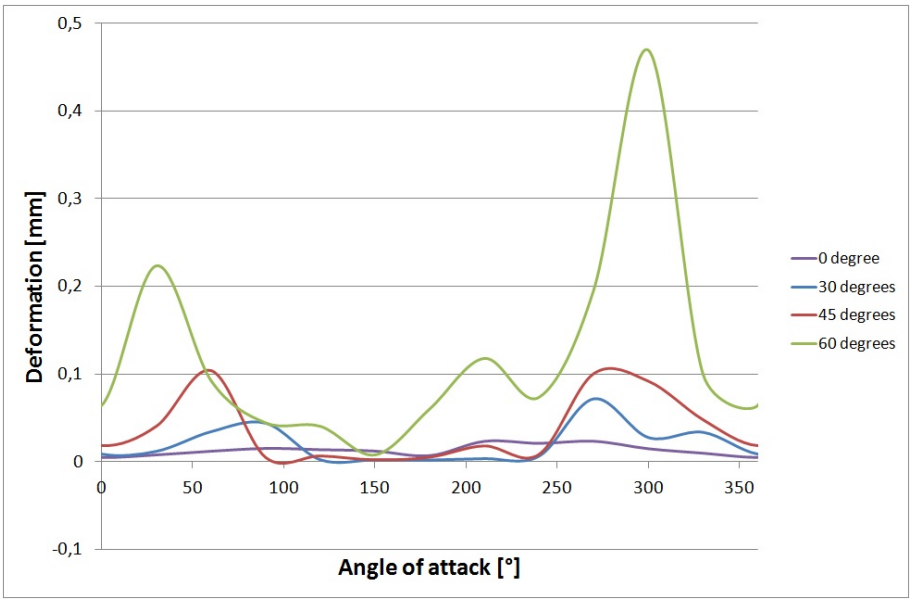

Figure 10.11: Deformation with respect to the angle of attack for a 60° closed valve

Concerning the maximum deformation, it represents 20% of the critical one, that is to say the minimum distance between the blade and the pipe wall. In the light of this result, the deformation should be considered as a matter of importance and a parameter that should be wise to try to diminish.

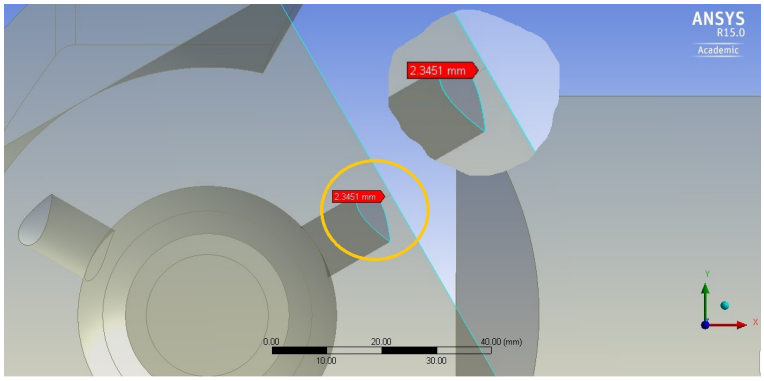

Figure 10.12: Minimum distance between blades and pipe

10.3 Hydrodynamic coefficients

Both hydrodynamic coefficients and moment that come out of these simulations have been investigated in order to understand how the valve closure influences the blades behavior that compose the turbine.

The main lesson learned form these charts is that these coefficients tend to be null for blades located in the "hidden area", that is to say where the fluid passing through the turbine has a lower influence. This area could be defined approximately (depending on the considered closure of the valve), as the range [100°;220°].

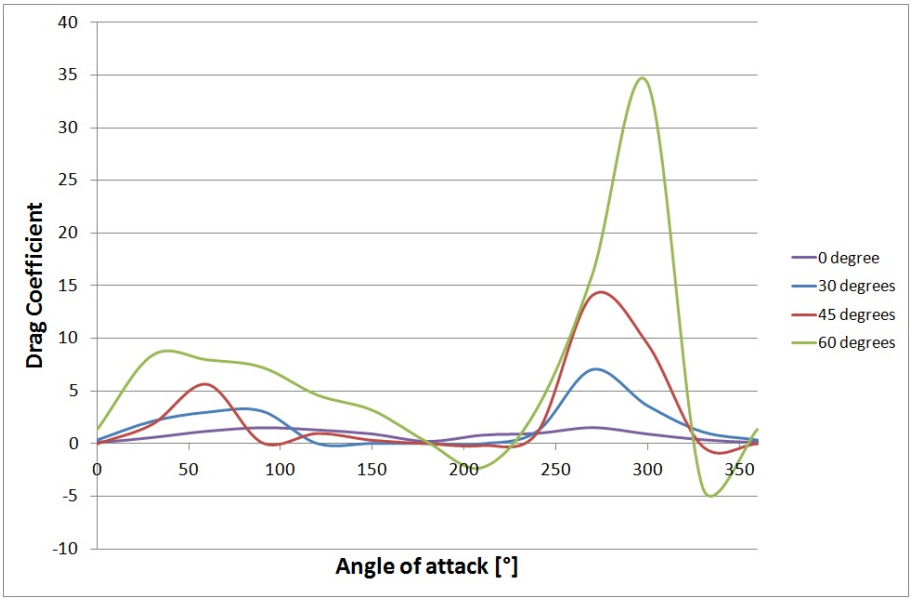

Figure 10.13: Drag coefficient for several valve closure angles

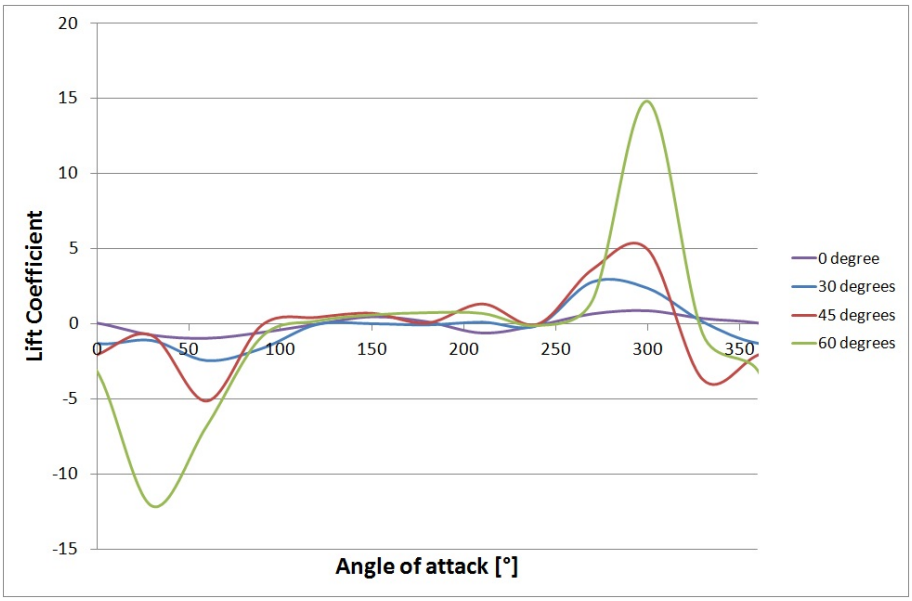

Figure 10.14: Lift coefficient for several valve closure angles

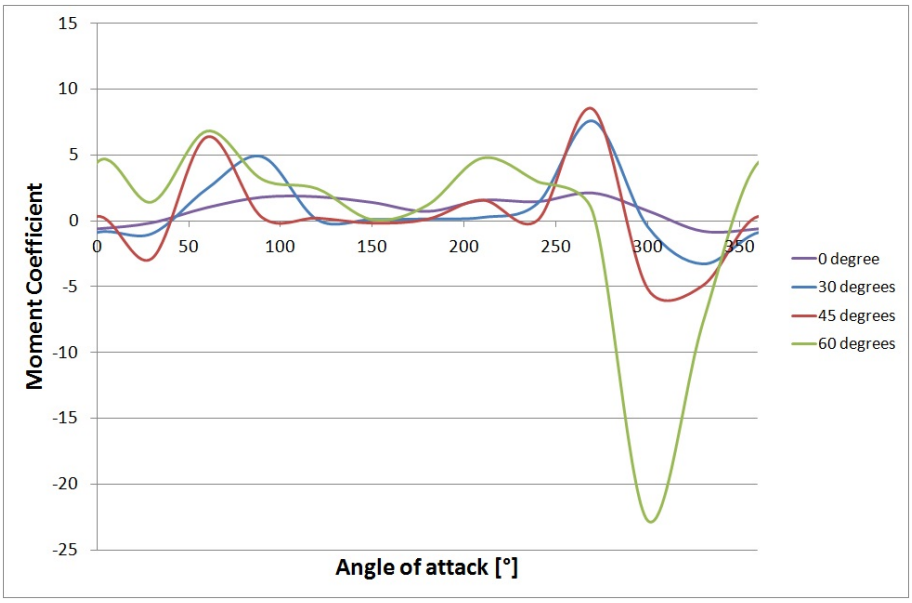

Figure 10.15: Moment coefficient for several valve closure angles

Consequently, as the fluid movement influence is reduced in a significant range, it will have a more important impact in the remaining range. This can be easily observed for the different parameters, as it creates a peak of values, more and more important, in a reducing range, as the valve is closing. Moreover, the evolution of the three structural parameters seems highly more influenced by the drag coefficient than by the lift one, as their curves have a similar trend of this one.

10.4 Flow coefficient C_v

The flow coefficient C_v is used to compare flow efficiency between valves, no matter their geometric differences.

In the following chart are presented C_v values with respect to the angle of attack, for the four cases previously considered. From this graph, one can observe that the more the turbine is closed, the lower is the C_v. In fact, when the turbine is fully opened, flow coefficient values oscillate between 420 and 375 $GPM/psi^{0,5}$. Progressively, when the aperture reduces, C_v values reduces as well, and the oscillation is less significant, up to a 60° valve closure, for which C_v is about 25 $GPM/psi^{0,5}$. Two informations can be extracted from these comments : the turbine efficiency decreases as it closes, and the more the turbine is closed, the less the position of the blades have an impact on the C_v value as it becomes constant with respect to the different angles considered.

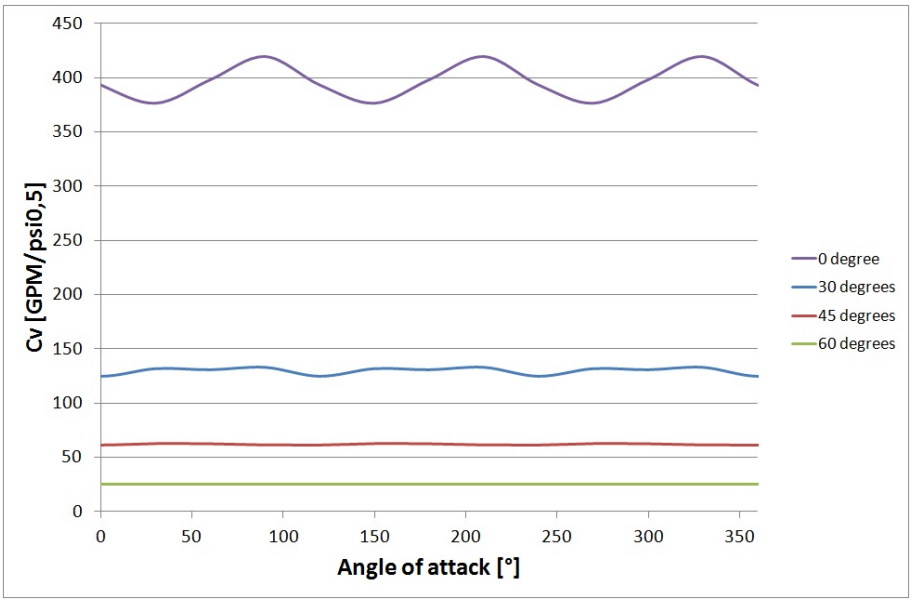

Figure 10.16: C_v values for several closing configurations

10.5 Modification of the fluid velocity inlet

In this first section, the fluid velocity inlet will be reduced for the most unfavorable case (Valve closure of 60° and angle of attack of 300°). The main goal is to plot a curve which shows the value of the Von Mises Stress with respect to the pressure drop Δp that appears due to the presence of the turbine.

Here are presented the results obtained for 6 several fluid velocity inlet values:

Velocity [m/s]	Von Mises Stress [MPa]	Equivalent Elastic Strain [-]	Total Deformation [mm]	Pressure drop Δp [Bar]
5	44,473	0,0213	0,4692	17,6410
4	26,335	0,0127	0,2908	10,9380
3	15,284	0,0074	0,1621	6,1897
2,5	11,31	0,0054	0,1129	4,2689
1	1,577	0,0008	0,0162	0,6737
0,5	0,4335	0,0002	0,0046	0,1693

Table 10.4: Maximum structural parameters values with respect to the fluid velocity inlet

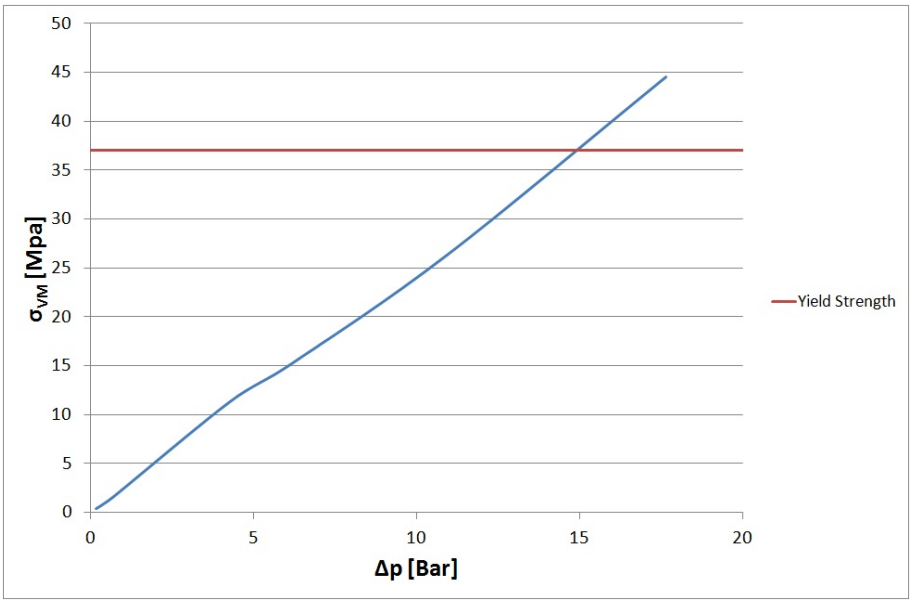

Figure 10.17: Maximum Von Mises stress with respect to the pressure drop Δp

The critical Von Mises stress is linearly linked to the pressure drop Δp, by the fonction $\sigma_{vm}(\Delta p) = 2,45 * \Delta p$. Equivalent Elastic Strain and deformation are also linearly linked to the pressure drop. It gives us a predictable tool to determine maximum values of these parameters by knowing the pressure drop, and shows that the system is highly influenced by its boundary conditions.

10.6 conclusion

To conclude, after being sure that the three dimensional model has the same behavior than the two dimensional one, and then the literature, the whole range of possible blades position has been investigated. The CFD-Structural interaction made possible to reach the Von Mises stress and strain, as well as the deformations of the structure.This let us conclude that the structure effectively resist to the constraints field created by the fluid going through the pipe. Then, several valve closure positions have been tested. As the valve must be able to closed itself, it ought to be designed to resist also to some fluid path modifications, due to the valve closure. As a matter of fact, the turbine was subjected to a such important stress field that it would damage it.

Due to this observation, alternate solutions will be developed in the following chapter.

Chapter 11

Alternative solutions to reduce stress field

After this first series of results, some modifications of several parameters, concerning the fluid velocity or the model geometry, will be made in order to see if it reduces the mechanical constraints on the turbine blades.

11.1 Reversal of the turbine's rotation direction

In this section, the position of the blades will be reversed. This means that the turbine will naturally spin in the other way and thus, it will be subjected to a whole new stress field, that will be examined and compared to the one previously studied. The most important point will be to see if the configuration is better or not in a structural point of view, especially concerning the maximum value of the Von Mises Stress, and consequently, the hypothetical yielding of material under the considered loading conditions.

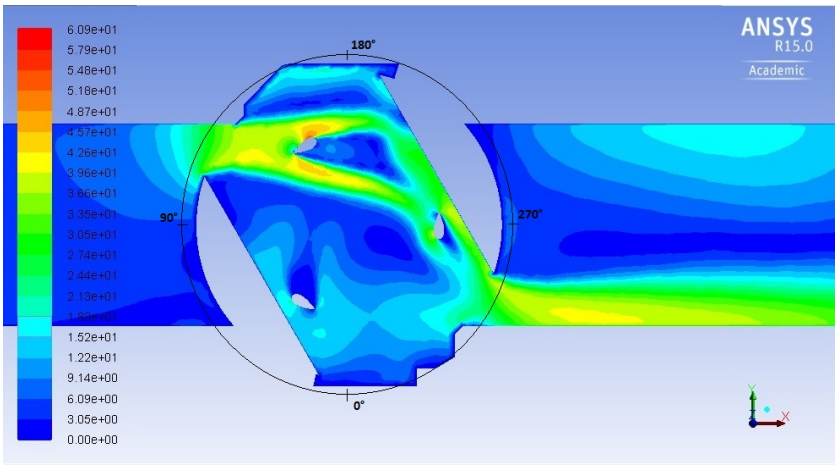

Figure 11.1: Velocity distribution inside the valve, considering a 60° closure angle, in the most unfavorable blades position

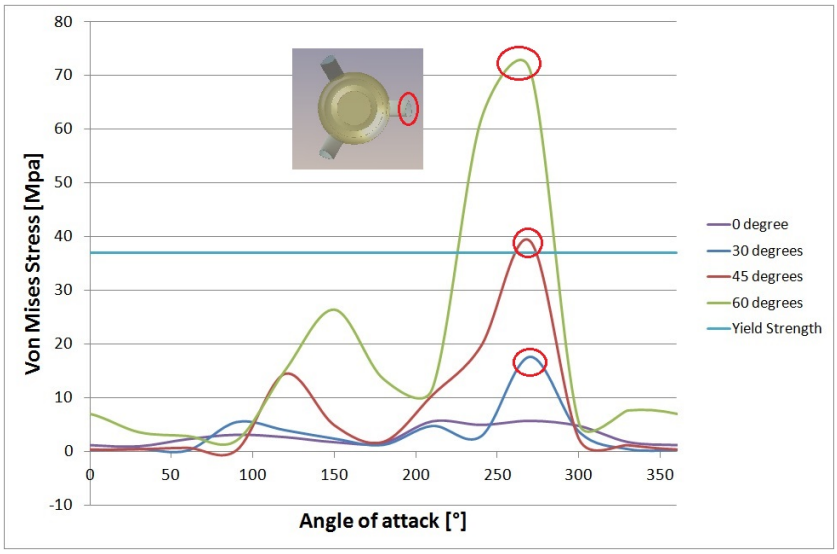

Figure 11.2: Von Mises stress with respect to the angle of attack of the reversed blades for the several closing configurations

In this configuration of the valve, it can be noticed that the value of the ultimate tensile strength (which is equal to 37 MPa), is more largely exceeded in this case than when the blades were oriented in the opposite direction. Moreover, this limit is not only exceeded when the valve is 60° closed, but only when the closure is equal to 45°.

In addition, it ought to be pointed out that the maximum Von Mises stress is not located around the leading edge, as in the original configuration, but in the trailing edge.

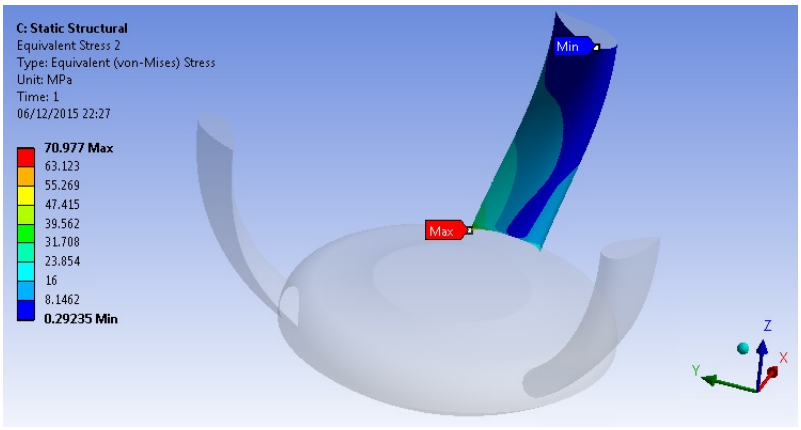

Figure 11.3: Maximum Von Mises stress location

This configuration is then more unfavorable than the one previously studied. To cope with this situation, it will be strengthened in its weakest part in order to reduce the stress field, and hopefully not overtake the ultimate tensile strength value.

11.2 Strengthening of the weakest part of the structure

In this second section, the geometry of the turbine will be slightly modified; It concerns the joint section between the blades and the base part. In fact, it has been observed, when the turbine spins clockwise, that no matter which blades position is considered, the maximum value of the Von Mises Stress is always located around this part. The choice has been made to soften this link in order to make it stronger.

In the following is presented the new geometry that will be experienced :

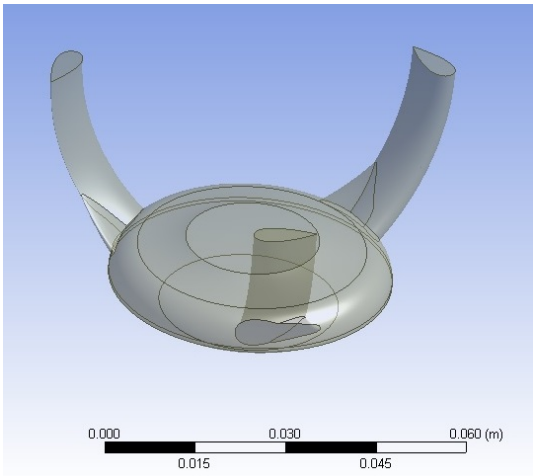

Figure 11.4: Strengthened turbine

Angle [°]	Max Equivalent Von Mises Stress [MPa]		Max Equivalent Elastic Strain [-]		Max Total Deformation [mm]	
-	Original	Modified	Original	Modified	Original	Modified
270	70,977	53,717	3,61E-2	2,69E-4	0,632	5,79E-3
150	26,427	17,869	1,41E-2	9,81E-5	0,239	2,51E-3
30	3,621	2,8488	1,69E-3	1,53E-5	0,037	4,39E-4

Table 11.1: Comparison between both geometries

By making the comparison between results obtained with both geometries, it clearly indicates that the new geometry experiences a much lower constraints field than the original one. For instance, the maximum Von Mises stress is reduced by about 25% with the new geometry. Even if its value of 53,717 MPa is still higher than the ultimate tensile strength, it needs to be taken into account that the fluid velocity inlet is still of 5 m/s, which is quite high. Moreover, about the Equivalent Elastic strain and the deformation,

these values are reduced by more than 100%.

In the following charts are respectively presented the distribution of stress and the deformation.

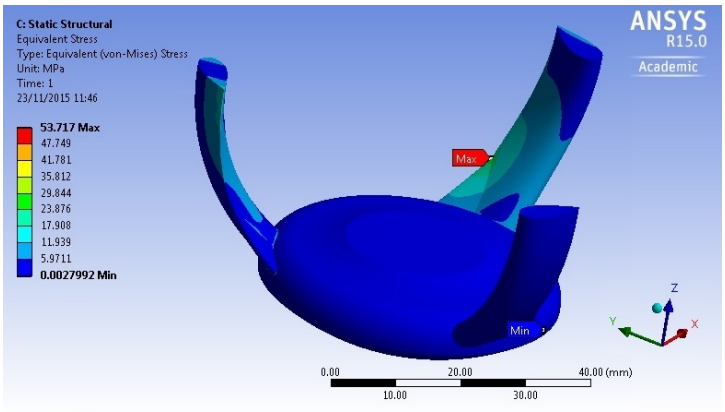

Figure 11.5: Von Mises stress for the new considered geometry

By taking a look to the Von Mises stress distribution, it can be noticed that its distribution has been modified. Not only its maximum value has been reduced, but it is not localized at the link between the blade and the base anymore; it takes place higher, in which would constitute the link between the blade and the new added part.

About the deformations experienced by the structure, the maximum value is still located in the middle part of the blade, but has been significantly reduced, due to the addition of the strengthening part. This can be explained by the fact that the deformation of a part depends directly on its distance from the fixed part. As the connection between the blades and the base has been made stronger by increasing the contact surface between those two parts, the blades won't be as deformed as they were in the previous case.

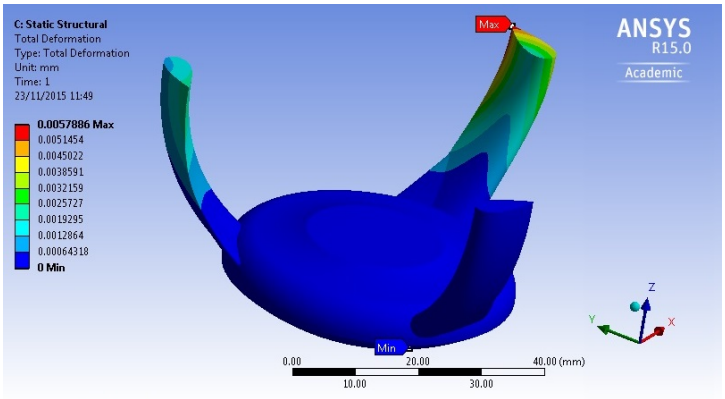

Figure 11.6: Deformation for the new considered geometry

11.3 Comparison between critical cases

An interesting point to develop would be the link between the pressure drop Δp and the maximum Von Mises stress value. The several configurations investigated along this chapter could bring some interesting informations about how which way to put the turbine inside the valve to reduce its structural damage.
In the following graph are presented 3 cases, which correspond to a 60° closed valve, in which the Von Mises stress is maximum. Yet, the position of the blade corresponding to the maximum stress is slightly different whether the turbine spins clockwise or counter-clockwise.

The original turbine position represents the turbine configuration that spins counterclockwise and which have been studied first. The maximum stress value is reached for α=300°.

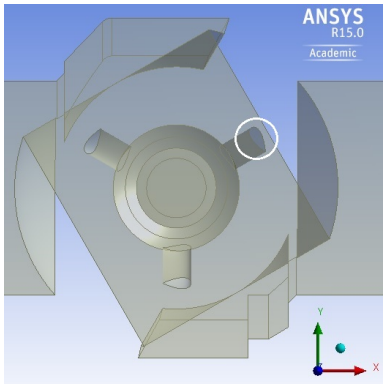

Figure 11.7: Original turbine position

Both following figures concern configurations for which the turbine has been reversed, it means it spins clockwise. It's for that configuration that the blades have been strengthened. In this case, the maximum stress value is reached for α=270°.

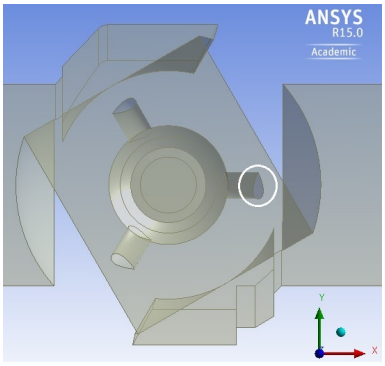

Figure 11.8: Reversed turbine

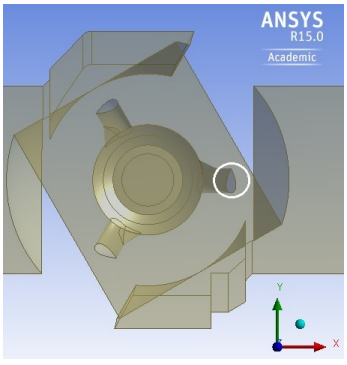

Figure 11.9: Reversed turbine strengthened

As the Von Mises stress linearly depends on the pressure drop Δp, the pressure drop,

which corresponds to the value for which the yielding strength value is reached, called Δp_{max}, can be easily obtained. These informations are summed up in the following chart.

	Δp [Bar]	Max Von Mises Stress [MPa]	Δp_{max} [Bar]
Original position	17,64	44,47	14,68
Reversed turbine	17,36	70,98	9,05
Reversed turbine with strengthened	16,76	53,72	11,54

Table 11.2: Maximum pressure drop Δp_{max} before yielding for each critical configuration

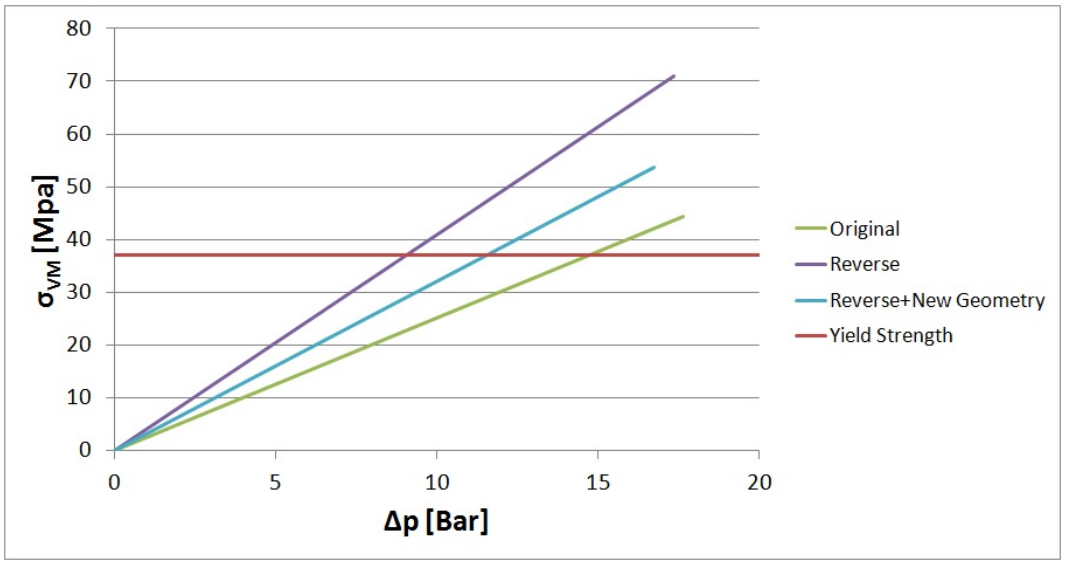

Figure 11.10: Maximum Von Mises stress with respect to the pressure drop Δp for the most critical configurations

It's interesting to notice that the configuration in which the turbine spins counterclockwise, can resist to an higher pressure drop than if it spins counterclockwise. That is still true even when the turbine is strengthened in its weakest part. Then, it seems that this position is the most favorable to resistant to the constrain field developed by the fluid acting on the turbine. Moreover, even if this configuration isn't opportune for the turbine to spins, it doesn't matter as the considered valve operates only on On and Off positions.

To conclude, the few modifications made in this chapter give a new perspective to the geometry used to design the turbine, and also its orientation inside the valve (Or equivalently, the valve closure direction). In fact, if the turbine has a counterclockwise spin direction, the constraints field, and the deformations experienced by this latter are smaller than if it spins clockwise (With the valve closure direction considered, *i.e.* clockwise). In the other hand, if it has been given to the turbine a clockwise spin direction (Which

seems more natural taking into account the valve closure direction), it is subjected to more constraints. One of the solution undertaken has been to modify the geometry, and more precisely the link between the blades and the base, which widely reduced the structural parameters values, but not enough to make it smaller to the one experienced in the original configuration.

Conclusion

This master thesis provides tools to understand the mechanisms that structurally influence a turbine placed in a pipe when a fluid is running through it. This project is constituted of two main parts.

The first one, concerning the CFD analysis, conducted through FLUENT, was performed in order to investigate the behavior of the fluid inside the pipe, the drag and lift coefficients, as well as the moment that is developed due to the relative motion between the fluid and the turbine; 12 positions of the blades which compose the turbine, and 4 closure angles have been taken into account.

Several conclusions can be made from this research : the confined environment has significant influence on the behavior of the blades, on the lift and drag coefficients, and on the moment developed by the turbine. On the other hand, the influence of the blades on each other remains relatively negligible.
Moreover, both 3D cases performed reveal that than the drag and lift coefficients have the same evolution (with respect to the angle of attack), no matter which case is considered (the 2D case is included in the same conditions in which the 3D ones have been performed, namely confined with the 3 blades, which corresponds to the configuration in which the GreenValve is willing to be exploited). This conclusion could make us consider a simplification of the problem's geometry to further explore, for instance, different turbines with more blades.

Once the CFD approach has been made, these results have been coupled to the structural part, that is to say the turbine, in order to see how the fluid behavior inside the pipe can impact the structural behavior of the turbine, and identify its most vulnerable parts.

The turbine is made of thermoplastic material, which enables a 3 dimensional print, in order to reduce manufacturing costs.

It can be observed, as expected, that as the valve is progressively closing, the stress field is concentrated in a specific zone inside the valve, which follows the fluid path, and makes the stress field significantly grow. From a certain point, which corresponds to few specific positions of the blades when the valve closure angle is equal to 60°, the Von Mises stress exceeds the ultimate tensile strength, which gives birth to irreversible deformations. Yet, the position for which is reached the maximum Von Mises stress changes along with the closure angle: this is linked to the modification of the flow path. This remark force us to consider alternatives such as a reinforcement of the weakest part of the turbine which significantly improves the way in which the turbine resists to constraints. It is also worth

noticing that the pressure drop and the maximum Von Mises Stress are linearly linked to each other, which makes possible to guess the maximum admissible pressure drop to prevent yielding.
It appears from this study that making the turbine spin in the opposite direction than the closing one better protects the latter.. In fact, the weakest part of the turbine is located in the joint between the blades and the turbine base, on its trailing edge.

Moreover, in order to decrease the maximum Von Mises stress, the shape of the NACA profile could be reconsidered, by using thinner one, in order to decrease values of the drag, which has a direct impact on the stress. Diminishing the maximum thickness of the NACA profile used for the GreenValve's turbine could constitute an interesting work in order to optimize the turbine's shape.

Finally, the geometry used all along this tesi, even if it is not the most appropriated to put in the GreenValve, constitutes a way to apprehend a new blade geometry, based on a NACA profile, different from what had been tested experimentally in laboratory.

Bibliography

[1] Stefano Malavasi, Giacomo Ferrarese, and Marco Maria Agostino Rossi. *A Control Valve for Energy Harvesting*. Elsevier Ltd, 2014.

[2] Stefano Malavasi, Giacomo Ferrarese, and Marco Maria Agostino Rossi. *Fluid-Dynamic Characterization of the GreenValve, an Energy Recovery Control Valve*. Politecnico di Milano, Departement of Civil and Environmental Engineering, 2014.

[3] L.X. Zhang, Y.B. Liang, X.H. Liu, Q.F. Jiao, and J. Guo. Aerodynamic Performance Prediction of Straight-Bladed Vertical Axis Wind Turbine Based on CFD, 2013. College of Mechanical and Electrical Engineering, Harbin Engineering University, China.

[4] Young-Tae Lee and Hee-Chang Lim. Numerical Study of the Aerodynamic Performance of a 500W Darrieus-Type Vertical-Axis Wind Turbine, 2015. School of Mechanical Engineering, Pusan National University, South Korea.

[5] Ion Malael[1] and Horia Dumitrescu[2]. Numerical Simulation of VAWT Flow Using Fluent, 2014. [1] Eng., Faculty of Aerospace Engineering, University Politehnica of Bucharest, [2] Prof., Institute of Mathematical Statistics and Applied Mathematics, Romanian Academy, Bucharest, Romania, ISSN 1454-2358.

[6] Franceso Balduzzi[a], Alessandro Bianchini[a], Riccardo Maleci[a], Giovanni Ferrara[a], and Lorenzo Ferrari[b]. Critical Issues in the CFD Simulation of Darrieus Wind Turbines, 2015. [a] Departement of Industrial Engineering, Univeristy of Florence, [b] CNR-ICCOM, National Research Council of Italy.

[7] J. Chen[a], H.X. Yang[a], C.P. Liu[b], C.H. Lau[b], and M. Lo[a]. A Novel VerticalAxis Water Turbine for Power Generation from Water Pipelines, 2013. [a] The Honk Kong Polytechnic University, Kowloonm Honk Kong, China, [b] Water Supplies Department, The Government of the Honk Kong SAR,China.

[8] Andrea Alaimo, Antonio Esposito, Antonio Messineo, Calogero Orlando, and Davide Tumino. 3D CFD Analysis of a Vertical Axis Wind Turbine, 2015. Faculty of Eingineering and Architecture, Kore University of Enna, Cittadella Universitaria, ISSN 1996-1073.

[9] Esteban Ferrer and Adeline Montlaur. *CFD for Wind and Tidal Offshore Turbines*. Springer, 2015.

[10] Jian Chen[a], Hongxing[b] Yang, and Mo Yang[a] Hongtao Xu[a]. The effect of the Opening Ratio and Location on the Performance of a Novel Axis Darrieux Turbine, 2015. [a] University of Shanghai for Science and Technology, China, [b] The Honk Kong Polytechnic University, Kowloon, Honk Kong.

[11] Mohammed Abdul Akbar and V. Mustafa. Regression Models for Predicting Force Coefficient of Aerofoils, 2015. Department of Civil Engineering, National Institute of Technology Calicut, NIT.

[12] Dipl.-Ing. Benjamin Lambie. Aeroplastic Investigation of a Wind Turbine Airfoil with Self-Adaptive Camber, 2011. Technischen Universitat Darmstadt.

[13] Abolfazi Pourrajabian[a], Peyman Amir Nazmi Afshar[b], Mehdi Ahmadizadeh[c], and David Wood[d]. Aero-Structural Design and Optimization of a Small Wind Turbine Blade, 2015. [a]Faculty of Aerospace Engineering, K.N. Toosi University of Technology, Tehran, Iran, [b]Department of Mechanical Engineering, Sharif University of Technology, Tehran, Iran, [c]Department of Mechanical Engineering, Shahrbabak Branch, Islamic Azad University, Shahrbabak, Iran, [d]Department of Mechanical and Manufacturing Engineering, University of Calgary, Calgary, Canada.

[14] Bjorn Roscher[a], Carlos Simao Ferreira[b], Lars Oliver Bernhammer[b], Helge Aagard Madsen[c], Daniel Todd Griffith[d], and Bernhard Stoevesandt[e]. Combined Structural Optimization and Aeroplastic Anlysis of a Vertical Axis Wind Turbine. [a]RWTH Aachen, Germany, [b]Delft University of Technology, Netherland, [c]DTU Wind Energy, Roskilde, Denmark, [d]Sandia National Laboratories, Albuquerque, USA, [e]Fraunhofer Institute, Oldenbourg, Germany.

[15] Abdullah Mobin Chowdhury[a], Hiromichi Akimoto[a], and Yutaka Hara[b]. Comparative CFD Analysis of Vertical Axis Wind Turbine in Upright and Titled Configuration, 2015. [a]Division of Ocean Systems Engineering School of Mechanical, Aerospace and Systems Engineering, Korea Advanced Institute of Science and Technology, South Korea, [b]Dept. of Mechanical and Aerospace Engineering, Graduate School of Engineering, Tottori University, Japan.

[16] Teresa Parra[a], Carmen Vega[b], A. Gallegos[c], N. C. Uzarraga[d], and F. Castro[a]. Design of H-Darrieus Vertical Axis Wind Turbine, 2015. [a]University of Valladolid, Spain, [b]University of Zulia, Venezuela, [c]University of Guanajuato, Mexico, [d]Technological University of Durango, Mexico.

[17] Kaman Aerospace Corporation. Design Study of Wind Turbines 50 kW to 3000 kW for Electric Utility Applications Analysis and Design, 1976. Prepared for NATIONAL AERONAUTICS AND SPACE ADMINISTRATION.

[18] K.M. Almohammadi[a,b], D.B. Ingham[b], L. Ma[b], and M. Pourkashanian[b]. Modeling Dynamic Stall of a Straight Blade Vertical Axis Wind Turbine, 2015. [a]Mechanical Engineering Department, Tiabha University, Saudi Arabia, [b]Centre for Computational Fluid Dynamics, Energy Technology and Innovation Initiative (ETTI), University of Leeds, Leeds.

[19] D.E. Calkins and D.L. Gray. An Experimental Investigation of the Two-Dimensional Hydrodynamic Characteristics of Bluff Symmetrical Fairing Sections, 1986. Department of Mechanical Engineering, University of Washington, Seattle.

[20] Alessando Bianchini[a], Francesco Balduzzi[a], John M. Rainbird[b], Joaquim Peiro[b], J. Michael R. Graham[b], Giovanni Ferrara[a], and Lorenzo Ferrari[c]. On the Influence of Virtual Camber Effect on Airfoil Polars for Use in Simulations of Darrieus Wind Turbines, 2015. [a]Department of Industriall Engineering, University of Florence, Italy, [a]Department of Aeronautical Engineering, Imperial Colloge, London, UK, [c]CNR-ICCOM, National Research Council of Italy, Sesto Fiorentino, Italy.

[21] J.M.R Gorle, S. Bardwell, L. Chatellier, F. Pond, M. Ba, and G. Pineau. PIV Investigation of the Flow Across a Darrieus Water Turbine, 2014. Institute PPRIME, ISAE-ENSMA, Poitiers, France.

[22] B. Roscher. *Structural Optimization of a Vertical Axis Wind Turbine with Aeroelastic Analysis*. PhD thesis, 2014.

[23] Gonabadi Hi, Moharrami N. andOila A., and Bull SJ. Wet Flexural Fatigue Behaviour of Tidal Turbine Blade Composite Materials. In *11th European Wave and Tidal Energy Conference*, 2015.

Appendix A

Velocity

In the following, first are presented a larger view of the three considered valve closure, in order to see how the fluid behaves once out of the valve. Moreover, figures corresponding to the several blades positions investigated, in which the velocity magnitude has been observed, are also presented.

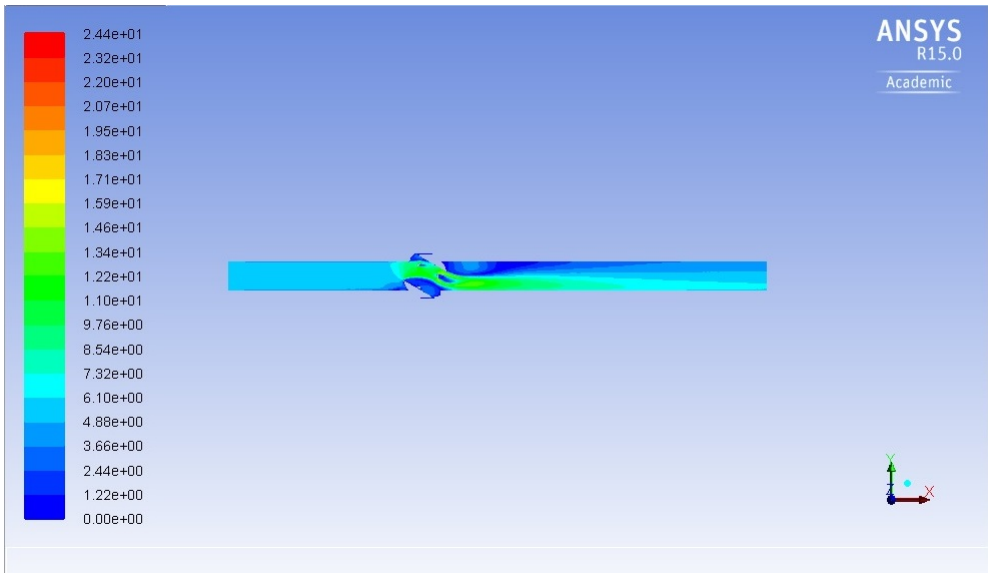

Figure A.1: Velocity inside the tube. Rotation sphere : 30°

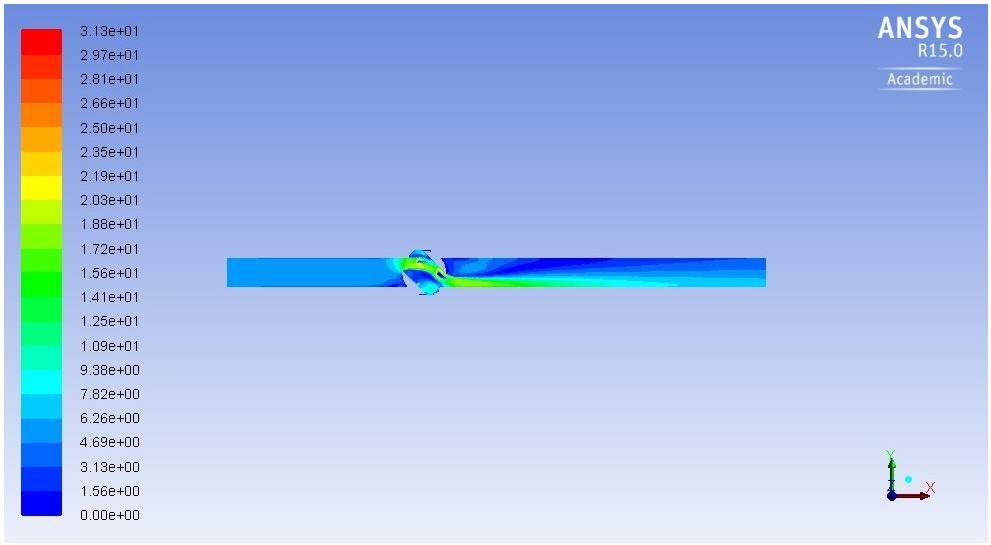

Figure A.2: Velocity inside the tube. Rotation sphere : 45°

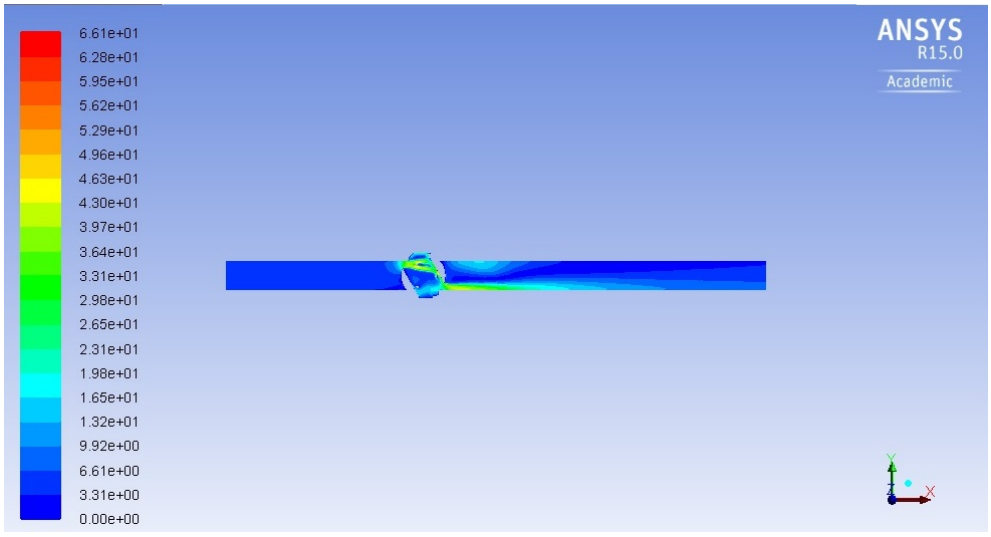

Figure A.3: Velocity inside the tube. Rotation sphere : 60°

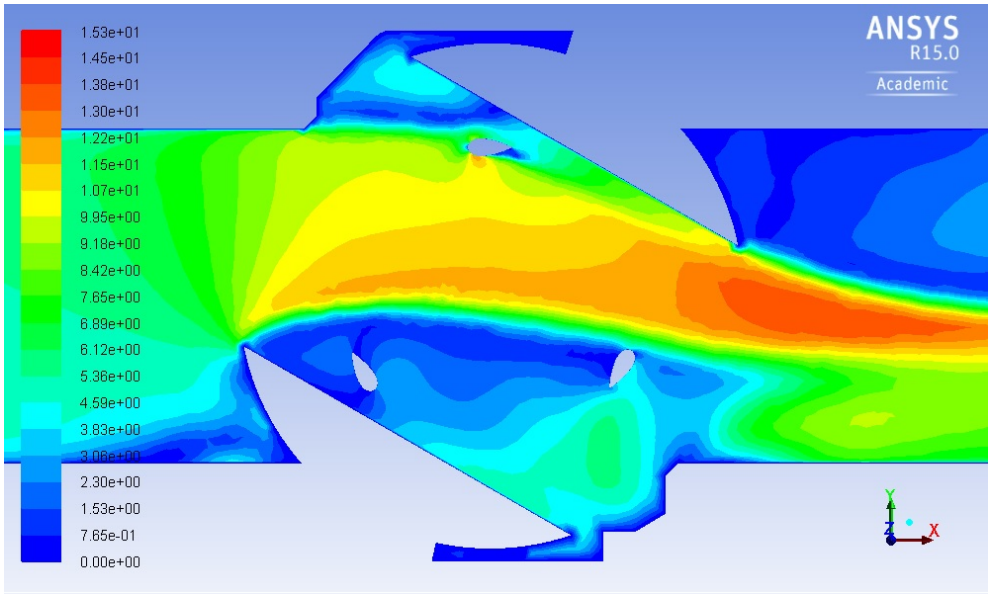

Figure A.4: Velocity inside the tube, focusing on the valve. Rotation sphere : 30˚, blades rotation : 0˚

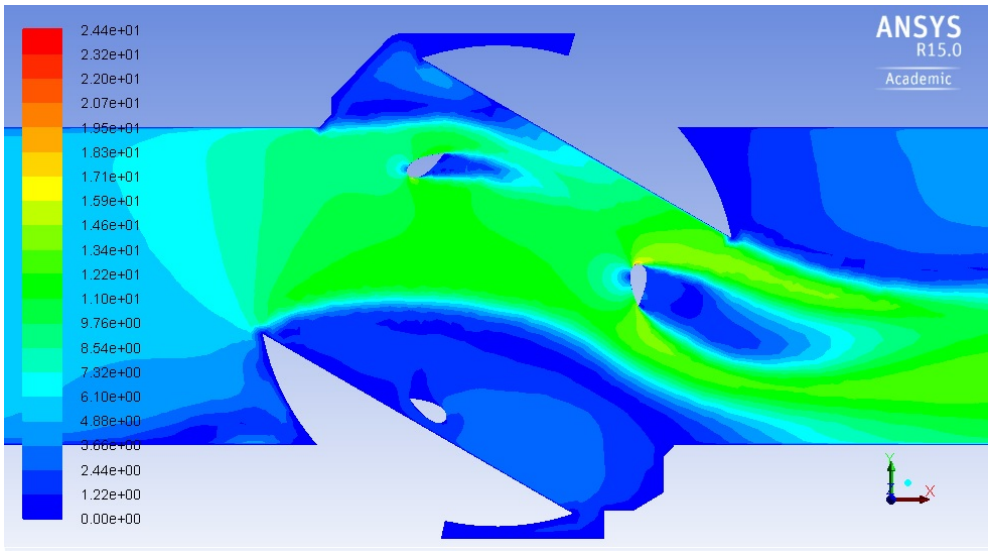

Figure A.5: Velocity inside the tube, focusing on the valve. Rotation sphere : 30˚, blades rotation : 30˚

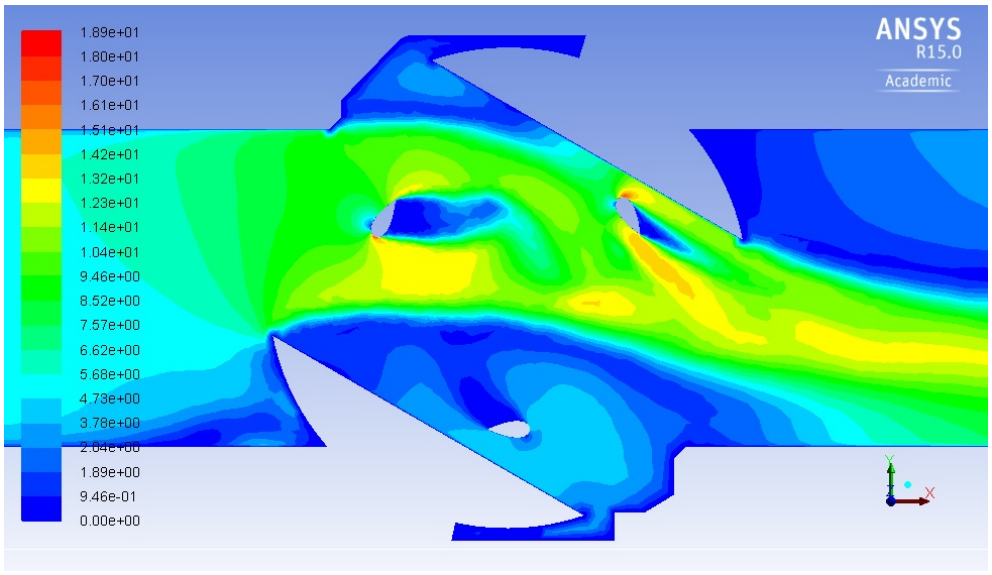

Figure A.6: Velocity inside the tube, focusing on the valve. Rotation sphere : 30°, blades rotation : 60°

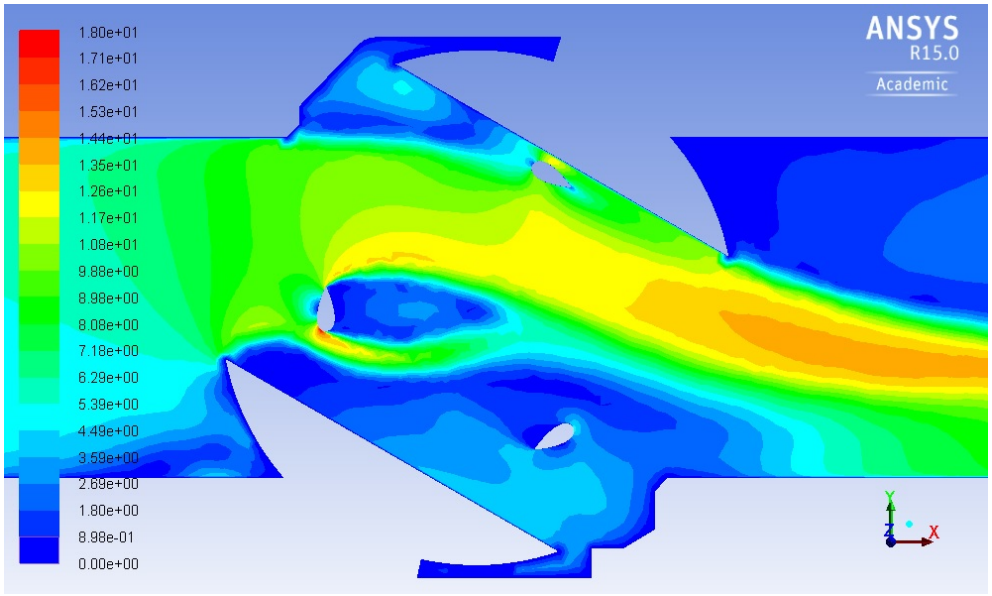

Figure A.7: Velocity inside the tube, focusing on the valve. Rotation sphere : 30°, blades rotation : 90°

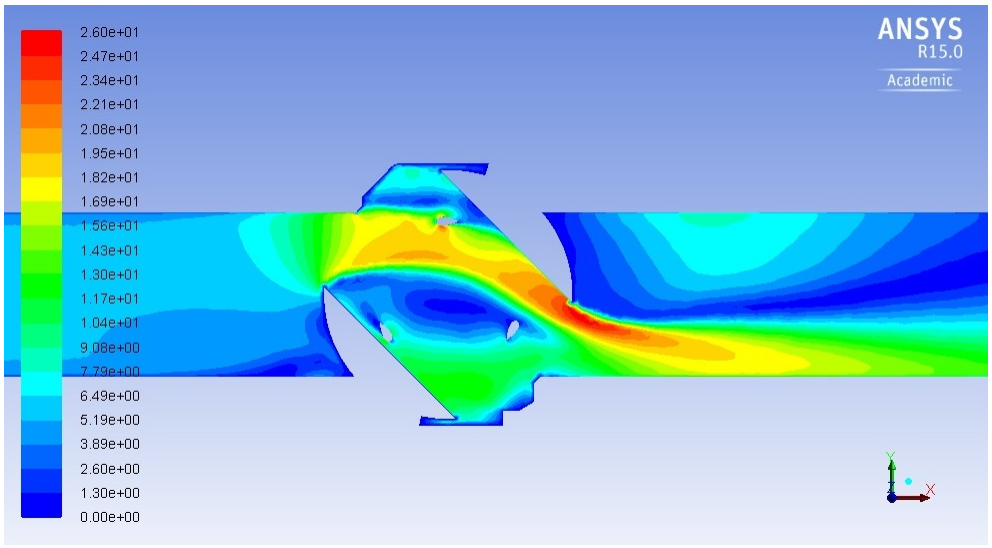

Figure A.8: Velocity inside the tube, focusing on the valve. Rotation sphere : 45°, blades rotation : 0°

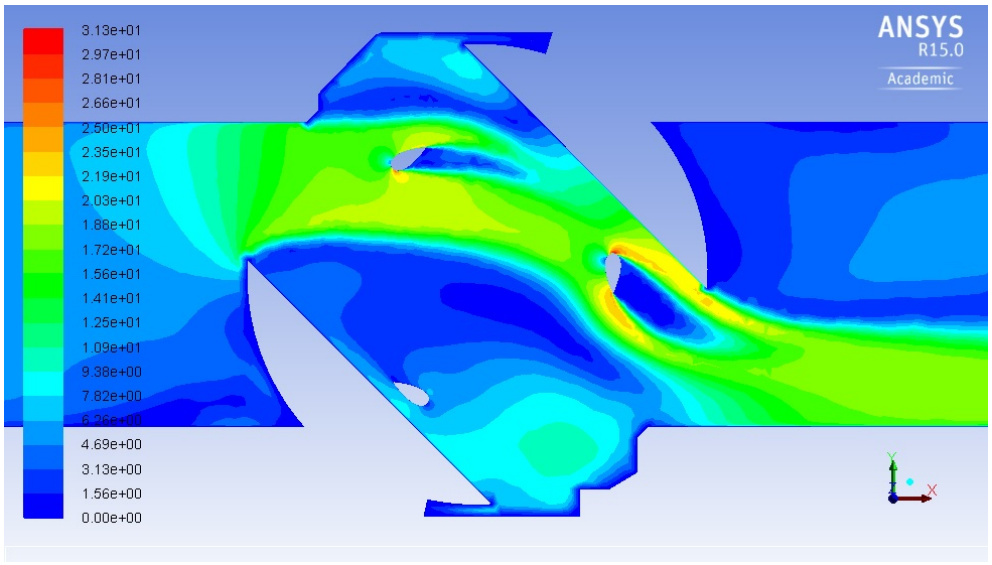

Figure A.9: Velocity inside the tube, focusing on the valve. Rotation sphere : 45°, blades rotation : 30°

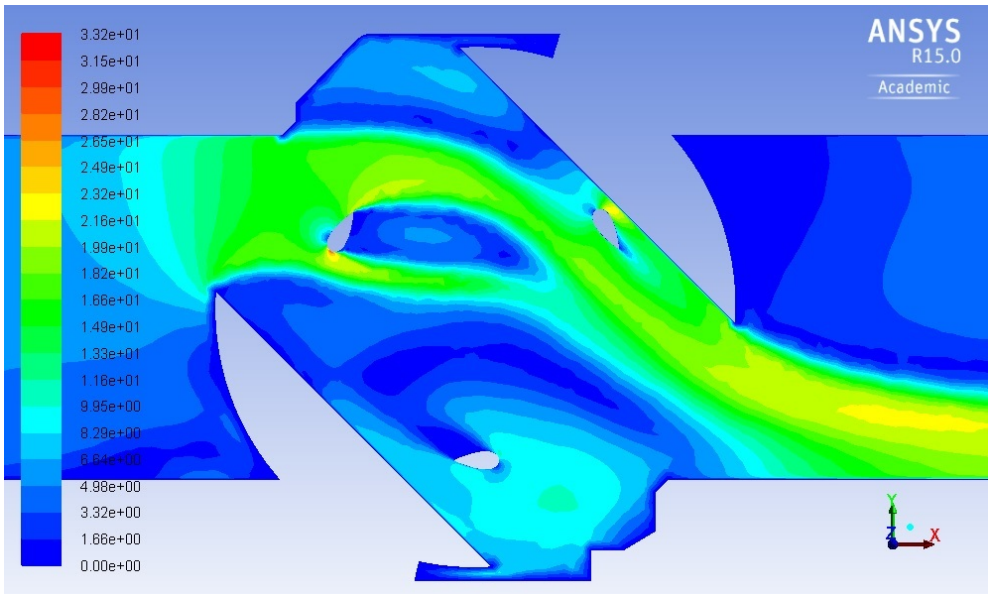

Figure A.10: Velocity inside the tube, focusing on the valve. Rotation sphere : 45˚, blades rotation : 60˚

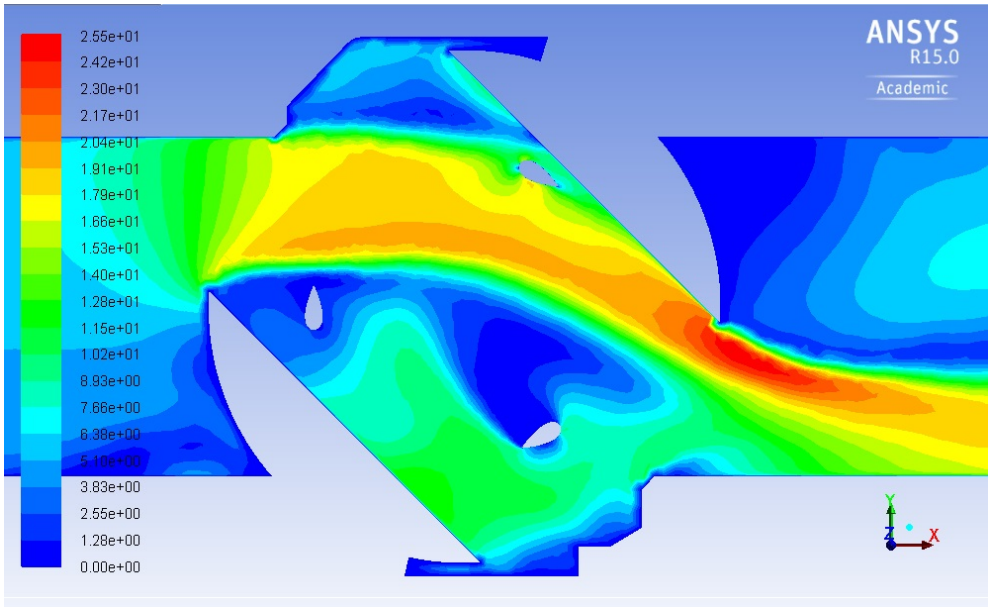

Figure A.11: Velocity inside the tube, focusing on the valve. Rotation sphere : 45˚, blades rotation : 90˚

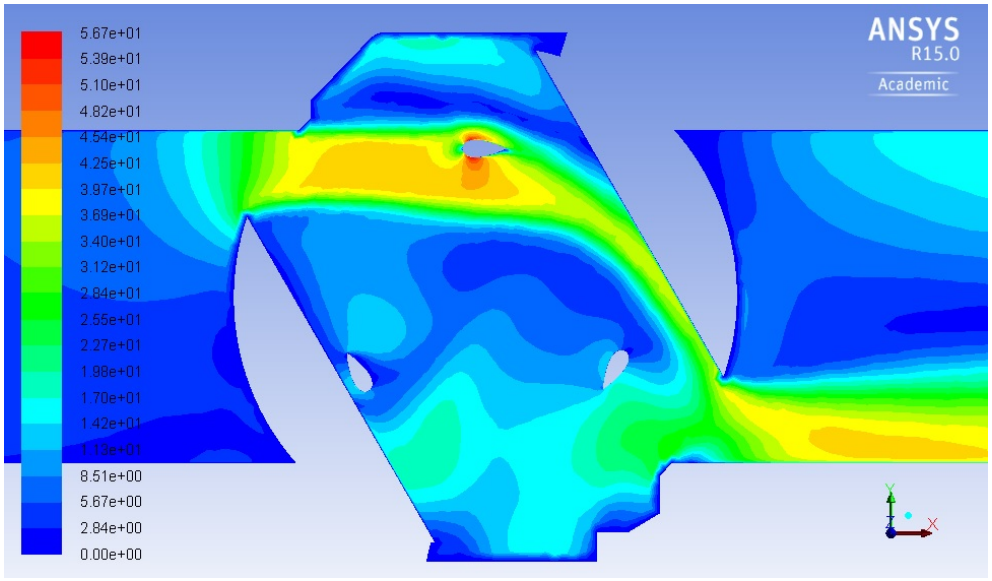

Figure A.12: Velocity inside the tube, focusing on the valve. Rotation sphere : 60˚, blades rotation : 0˚

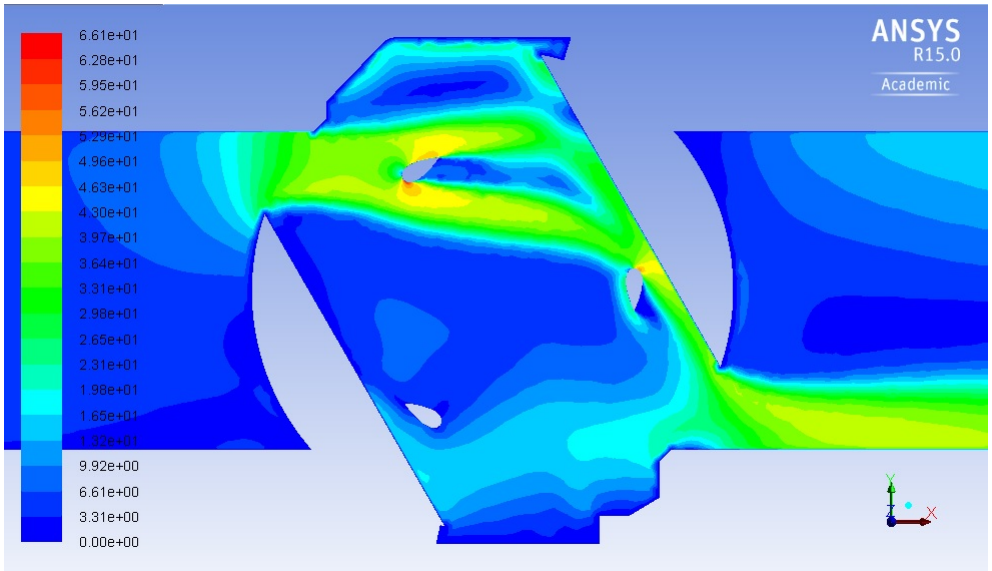

Figure A.13: Velocity inside the tube, focusing on the valve. Rotation sphere : 60˚, blades rotation : 30˚

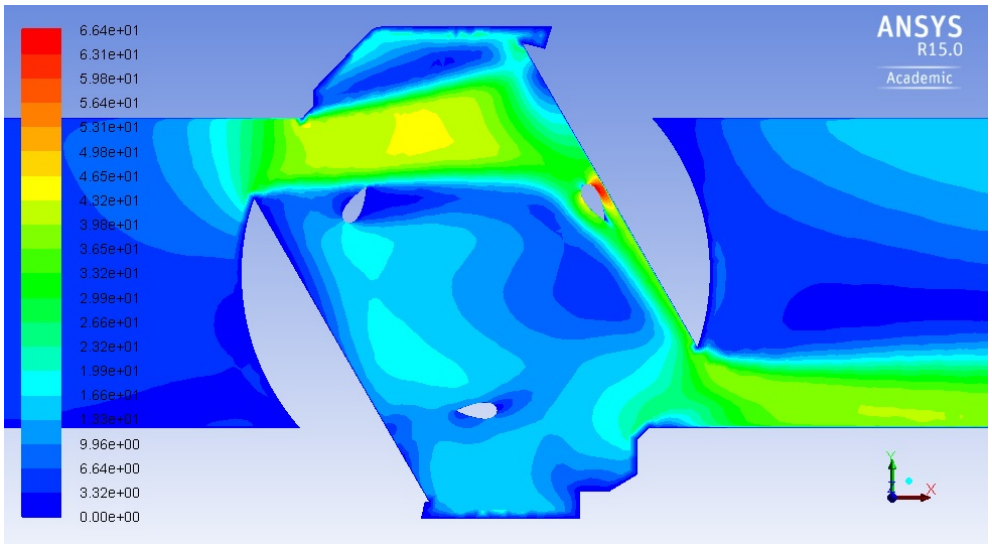

Figure A.14: Velocity inside the tube, focusing on the valve. Rotation sphere : 60˚, blades rotation : 60˚

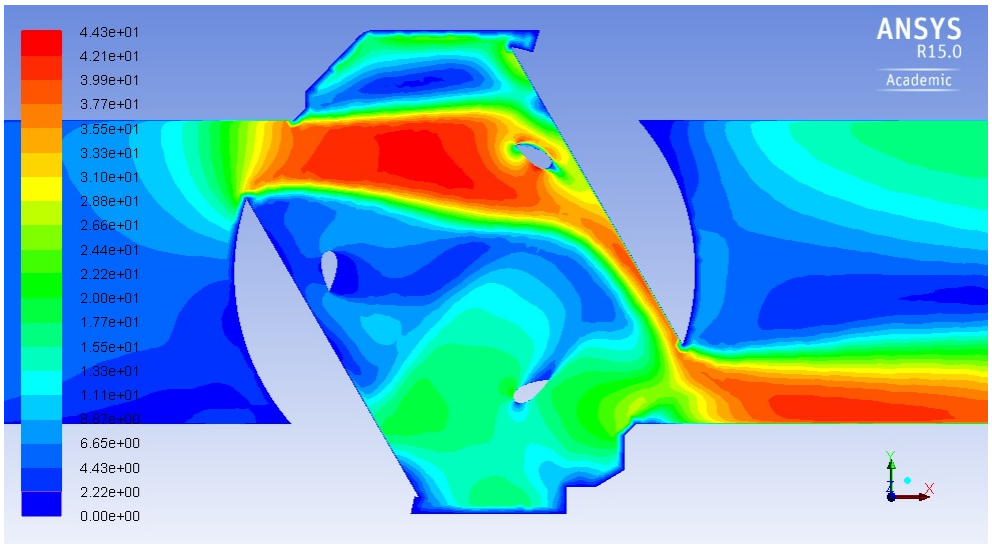

Figure A.15: Velocity inside the tube, focusing on the valve. Rotation sphere : 60˚, blades rotation : 90˚